SUPPORT INFORMATION

Solid-to-Liquid Mechanochemistry: Multiscale Synthesis of Electrochemically Relevant Ionic Liquids

Felipe Machado, Roberto M. Torresi* and Paulo F. M. Oliveira*

Institute of Chemistry, University of São Paulo, Av. Prof. Lineu Prestes 748, 05508-000 São Paulo, Brazil.

*Corresponding author. E-mail address: rtorresi@iq.usp.br (R.M.T.), paulofmo@usp.br (P.F.M.O.)

1. Materials and methods

1.1. Materials

Sodium bis(fluorosulfonyl)imide (NaFSI, 99.9 %, Solvionic), sodium bis(trifluoromethanesulfonyl)imide (NaTFSI, 99.5 %, Solvionic), sodium trifluoromethanesulfonate (NaTfO, 98%, Sigma-Aldrich), 1-butyl-1-methylpyrrolidinium bromide ($Pyr_{14}Br$, 99 %, Ionic Liquids Technologies), 1-butyl-1-methylpiperidinium bromide ($Pip_{14}Br$, 99%, Ionic Liquids Technologies), 1-butyl-2,3-dimethylimidazolium bromide (BDMImBr, 99%, Ionic Liquids Technologies), 1-butyl-1-methylpyrrolidinium bis(fluorosulfonyl)imide ($Pyr_{14}FSI$, 99.5 %, Solvionic), 1-butyl-1-methylpyrrolidinium bis(trifluoromethanesulfonyl)imide ($Pyr_{14}TFSI$, 99.5 %, Solvionic), hexadeuterodimethyl sulfoxide (DMSO-d^6, 99.9 atom % D, Sigma-Aldrich), dichloromethane (Synth Brazil) and deionized water.

1.2. Synthesis of Ionic Liquids

Planetary Ball Milling. Equimolar amounts of $Pyr_{14}Br$, $Pip_{14}Br$, and BDMImBr were combined with NaX (X = TfO, TFSI, or FSI) under solvent-free conditions in a Pulverisette 7 Premium line (Fritsch®) planetary ball mill, using a jar and spheres (⌀ = 10 mm) made of Si_3N_4. After milling, NaBr was removed from the liquid phase (dichloromethane and IL mixture) using MultiGE filtration units. The volume of dichloromethane used was 20 mL per synthesis. The solid residue was oven-dried at 60 °C for 24 h before XRD analysis. The ionic liquids were recovered from by rotary evaporation (Büchi R-215) under reduced pressure (<30 mbar) at 60 °C for 2 h. Milling speeds ranged between 250 and 720 rpm, with total milling times from 20 to 640 min. Each experiment was conducted through

successive 15 min grinding cycles, with 5 min pauses to avoid overheating and IL degradation. For instance, milling at 500 rpm over 240 min required 16 consecutive grinding cycles (16 x 15+5 min). For hydrophobic ionic liquids, purification was required to reduce the Br^- content. The ILs were washed with 50 mL of water per cycle, for a total of four washings (200 mL in total). A control experiment was performed with $Pyr_{14}Br$ and NaTFSI, in which ~2.35 g of the reagents were mixed in stoichiometric proportions without mechanical agitation. The mixture was prepared and maintained inside a glovebox under an argon atmosphere with low moisture content. The vessel was sealed, and the mixture was monitored over one week (Video S1).

Planetary Mixer. Equimolar amounts of Pyr14Br (41.98 g) and NaTFSI (57.28 g) were combined under solvent-free conditions using a GELON planetary mixer (GL-S100F). The blade rotation speed was set to 500 rpm, and mixing was carried out under vacuum. The dimensions of the vessel and blades are shown in **Figure S31**. Most details can be viewed in **Video S2**. At 30-minute intervals, the system was briefly opened to collect small aliquots for visual monitoring of the reaction progress. The samples collected were centrifuged at 11,000 rpm for 30 minutes. After 360 minutes of reaction, dichloromethane was added (V = 50 mL) to dissolve the IL and facilitate the removal of NaBr by filtration. The IL was subsequently washed with distilled water (50 mL per washing, four in total), following a procedure analogous to that employed in ball-milling synthesis. Finally, the reaction precipitates were dried in a vacuum oven at 60 °C for 24 hours prior to XRD analysis.

Yield and conversion. The yield and conversion of the syntheses were determined according to equations (1) and (2). Conversion was calculated with respect to the starting material serving as the cation source, n_i, specifically those precursors bearing bromide as the counterion. The residual amount of unreacted starting material, n_f, was estimated based on the bromide content measured in the final product by ion chromatography, using samples of the ILs that were not subjected to aqueous washing. The yield was used in equation 2 to compensate for the initial mass loss. If it is not used, the calculation will be overestimated because it will assume that there will be no mass loss.

$$Yield\ (\%) = \frac{mass_{IL}\ exp}{mass_{IL} theorical} * 100 \quad (1)$$

$$X\ (\%) = \frac{n_i * yield - n_f}{n_i * yield} * 100 \quad (2)$$

1.3. Characterization

X-ray diffraction (XRD). The XRD technique was used to identify the crystal structure of the precipitate formed during the mechanochemical synthesis of ILs. XRD patterns were recorded in a Shimadzu XRD-7000 MAXima diffractometer, using Cu Kα radiation, over an angular range of 10 – 80° with a step size of 0.02 s^{-1}.

Ion chromatography (IC). The IC technique was used to quantify the bromine content in the synthesized ionic liquids. Measurements were carried out on a 761 SD Compact IC (Metrohm) chromatograph, equipped with an anion exchange column (Metrosep A Supp 4, 250/4.0 mm, Metrohm) and suppressor. The quantification method was adjusted based on the work developed by Villagrán et al.[1] and Hao et al.[2]. A 4mM carbonate/sodium bicarbonate solution (pH ~ 10) was used as the eluent phase. Approximately 0.12 g of sample was dissolved in water (hydrophilic IL) or in a 50:50 v/v water-acetonitrile mixture (hydrophobic IL). Calibration curves were constructed with the precursors $Pry_{14}Br$, $Pip_{14}Br$, and BDMImBr with concentrations between 10 - 1000 ppm. The retention time of Br^- on the column is ~ 340 – 350 s. The calibration curve with the standards is available in Figures S4–6. Chromatograms of all ILs synthesized via mechanochemistry are presented in **Figures S5–9.**

Inductively Coupled Plasma Optical Emission Spectrometry (ICP-OES). The determination of sodium content in samples of ionic liquids synthesized by mechanochemistry was performed by ICP-EOS (Agilent spectrometer model 5800). The samples were prepared with nitric acid and heated in a digestion block at 100ºC in closed bottles.

Nuclear Magnetic Resonance (NMR). NMR spectroscopy was used to analyze the chemical identity of the synthesized ILs and their purity. ^1H and ^{13}C NMR spectra were collected on a Bruker AIII 300 MHz spectrometer, using DMSO-d^6 as solvent. The NMR spectra was collected after the dichloromethane removal step by rotary evaporation. All data was processed with the aid of MestReNova® software. The spectra ^1H NMR for the cation source precursors are available in **Figures S11-13**. NMR spectra of ILs are presented in **Figures S14-23**.

Karl-Fisher Coulometric Titration. KF titration technique was used to determine the water content in the synthesized ionic liquids. Measurements were performed on a KF899 Coulometer (Metrohm). All samples were previously heated at 50 – 80 ºC for several days inside the glovebox with water content ≤ 5 ppm before measurements. The H_2O quantifications were carried out before the FTIR measurements, physicochemical

and electrochemical properties. The water contents obtained were ≤ 10 ppm after drying in glovebox.

Fourier Transform Infrared Spectroscopy (FTIR). Attenuated Total Reflectance Fourier Transform Infrared Spectroscopy (ATR-FTIR) was performed on Bruker Vertex 80v spectrometer with a frequency range from 400 to 4000 cm^{-1} under vacuum (< 2 hPa) . All spectra were collected with a resolution of 4 cm^{-1} and 64 scans. Before measurements, the ionic liquids were heated at 100 ºC for 48 h to remove water inside the glovebox.

Thermogravimetric Analysis (TGA) and Differential Scanning Calorimetry (DSC). The thermal stability was verified by TGA – Q500 equipment (TA Instruments). The samples (5 – 8 mg) were handled and weighed in a dry room. Each sample was measured in the temperature range of 25 to 550 °C at a heating rate of 20 °C min^{-1}. During the tests, synthetic air or nitrogen was flown at a 150 ml min^{-1} flow rate. In turn, the transitions and phase changes were verified via differential scanning calorimetry (DSC). All measurements were performed using a thermal analyzer system TA Instruments Q20 DSC at a heating rate of 10 °C min^{-1} in the temperature range of −80 to 60 °C. Samples were hermetically sealed in an aluminum crucible in an argon-filled glovebox. For all samples subjected to heating, cooling and reheating, in this order.

Ionic Conductivity, Viscosity and Density. Ionic conductivities of ILs were determined by Electrochemical Impedance Spectroscopy (EIS) using a Autolab PGSTAT 30 (Metrohm) in the frequency range from 10 kHz to 10 Hz, at a varying temperature from 298.15 to 348.15 K. The measurement was conducted using the Micro cell HC (RHD 80014, Metrohm) with two Pt electrodes and temperature control. The cell constant was determined using standard KCl solutions (0.001, 0.01 and 0.1 mol L^{-1}). Viscosity and density of ILs were measured with a viscometer-densimeter (SVM 3000; Anton Paar) from 298.15 to 348.15 K at atmospheric pressure. All ILs were kept under heating for several days at 80 °C, except $Pyr_{14}FSI$ (50 °C), inside a glovebox with water content below 5 ppm. The experimental data for conductivity and viscosity as functions of temperature were fitted using the Vogel–Tammann–Fulcher (VTF) equation (equation 3 and 4), which is widely employed for describing the behavior of ionic liquids: [3–5]

$$\sigma = \sigma_0 \exp\left(\frac{-B}{T-T_0}\right) \quad (3)$$

$$\eta = \eta_0 \exp\left(\frac{B}{T-T_0}\right) \quad (4)$$

where σ_0, η_0, B and To are adjustable parameters. Here, the T_o values employed in the fitting procedure were fixed and selected based on the T_g of pure ionic liquids

reported in the literature. The T_o values adopted were 188.15 K[6], 169.15 K[6], 192 K[4], 200.15 K[7] and 198.15 K[8] for Pyr_{14}TFSI, Pyr_{14}FSI, Pyr_{14}TfO, Pip_{14}TFSI, and BDMImTFSI, respectively. In turn, the density of the ILs was further estimated using the empirical equation proposed by Ye and Shreeve[9]:

$$\rho_{calc} = \frac{\mathrm{W}}{0.6022\ \mathrm{V}} \quad (5)$$

where W represents the molar mass and V the sum of the estimated molecular volumes of the cation and anion. For these calculations, the adopted ionic volumes were 253 Å^3 (Pyr_{14}^+)[9], 271 Å^3 (Pip_{14}^+)[3], and 270 Å^3 ($BDMIm^+$)[10] for the cations, and 248 Å^3 ($TFSI^-$)[9] and 139 Å^3 (FSI^-)[11] and 129 Å^3 (TfO^-)[9] for the anions.

Linear sweep voltammetry (LSV). The electrochemical windows stability (ESW) was performed by LSV at 5 mV s^{-1} and room temperature. The experiment utilized a Swagelok type cell (T Shape) equipped with aluminum/active carbon discs (working electrode) and active carbon (counter electrode), both with ⌀ = 12 mm. A silver/silver chloride wire was used as the reference electrode. The electrodes were separated by glass fiber discs (⌀ = 12 mm). The cell was assembled and sealed inside a glovebox with a water content of less than 5 ppm. The measurements started with the determination of the open circuit potential, then an electric current was applied until the current density reached ± 150 μA cm^{-2}. Measurements were performed on an Autolab PGSTAT 30 (Metrohm). The potentiodynamic i/E curves were obtained separately from the OCP to more negative or positive potentials.

E-factor measurements. In this work, the simple E-factor (sEF), standard E-factor (EF), and complete E-factor (cEF) were estimated to assess the sustainability of the mechanochemical synthesis and IL production process. The mass of the solvent and water was estimated from their density at 25 °C. The equations for each metric are given below:

$$sEF = \frac{\Sigma\, mass\ of\ reagents - mass\ of\ desired\ product}{mass\ of\ desired\ product} \quad (6)$$

$$EF = \frac{\Sigma\, mass\ of\ reagents + \Sigma\, mass\ of\ solvent - mass\ of\ desired\ product}{mass\ of\ desired\ product} \quad (7)$$

$$cEF = \frac{\Sigma\, mass\ of\ reagents + \Sigma\, mass\ of\ solvent + \Sigma\, mass\ of\ water - mass\ of\ desired\ product}{mass\ of\ desired\ product} \quad (8)$$

2. Characterization

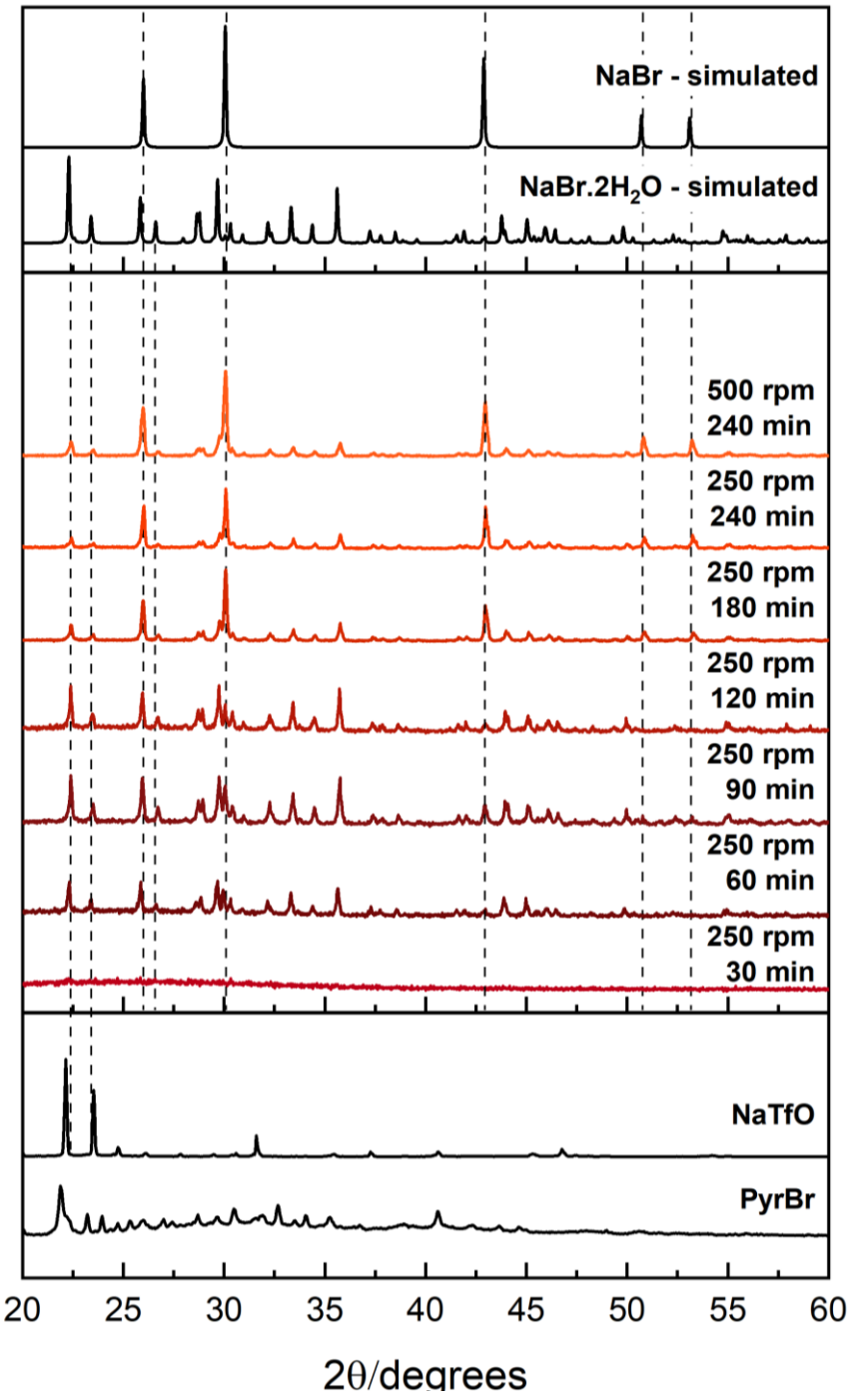

Figure S1. PXRD patterns of the solid product formed during the synthesis of $Pyr_{14}TfO$ IL as function of milling conditions.

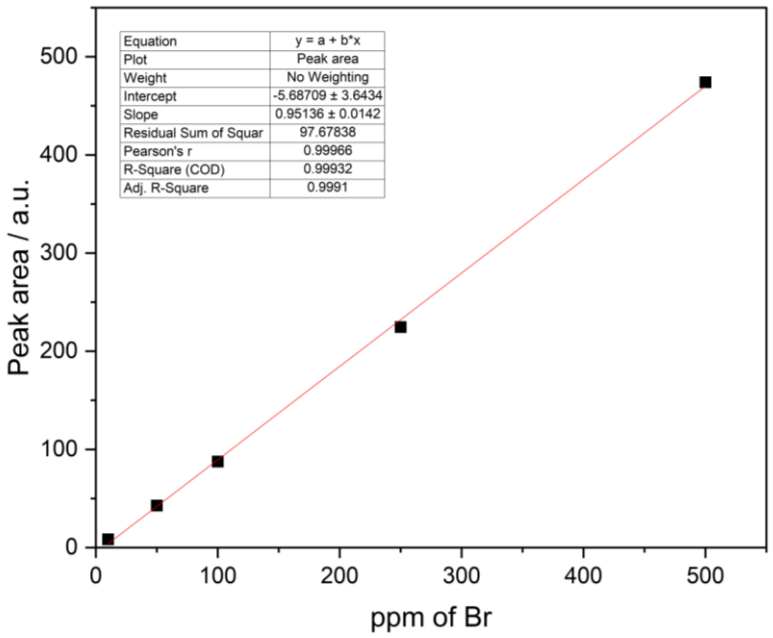

Figure S2. Calibration curve of Br from $Pyr_{14}Br$ using an eluent 4 mM carbonate/sodium bicarbonate solution and a flow rate of 1 mL min^{-1} during 20 min.

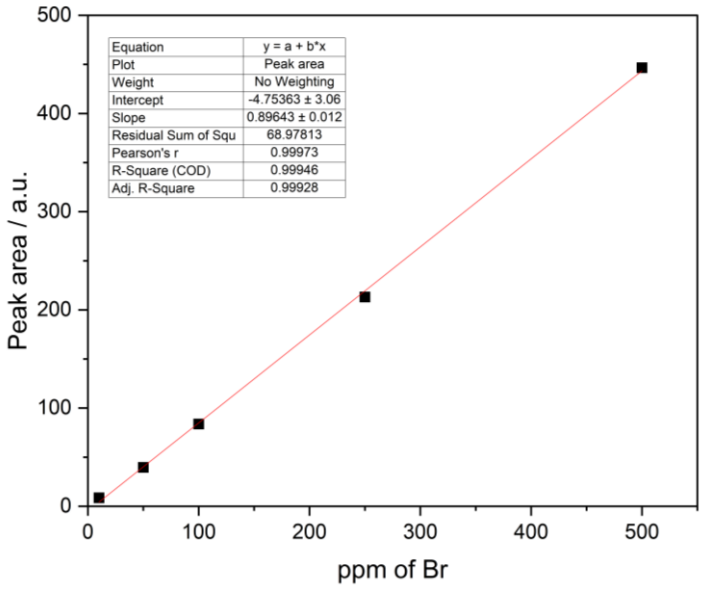

Figure S3. Calibration curve of Br from $Pip_{14}Br$ using an eluent 4 mM carbonate/sodium bicarbonate solution and a flow rate of 1 mL min^{-1} during 20 min.

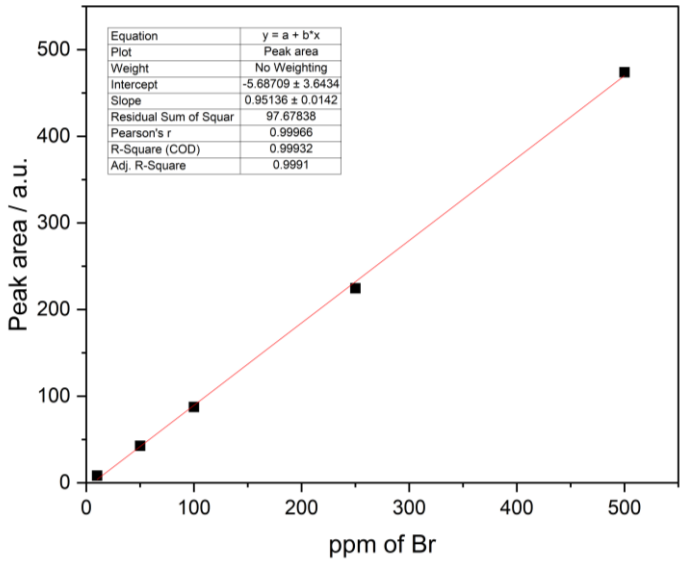

Figure S4. Calibration curve of Br from BDMImBr using an eluent 4 mM carbonate/sodium bicarbonate solution and a flow rate of 1 mL min^{-1} during 20 min.

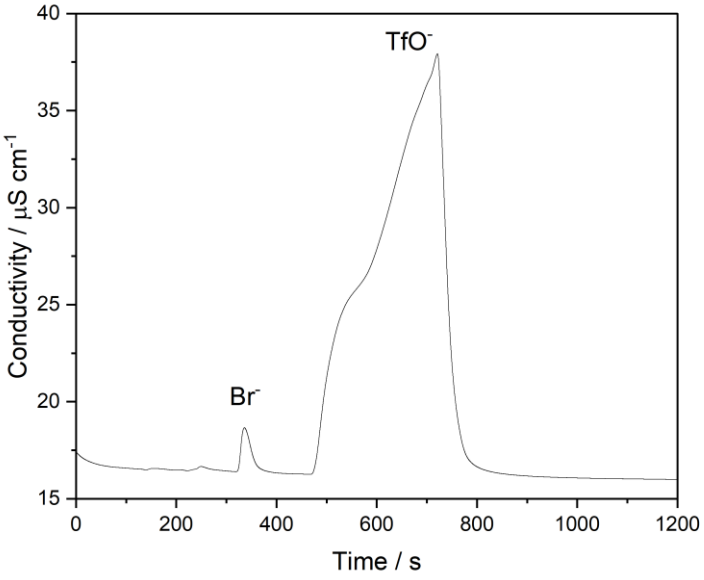

Figure S5. Ion chromatogram of $Pyr_{14}TfO$ using an eluent 4 mM carbonate/sodium bicarbonate solution and a flow rate of 1 mL min^{-1} during 20 min.

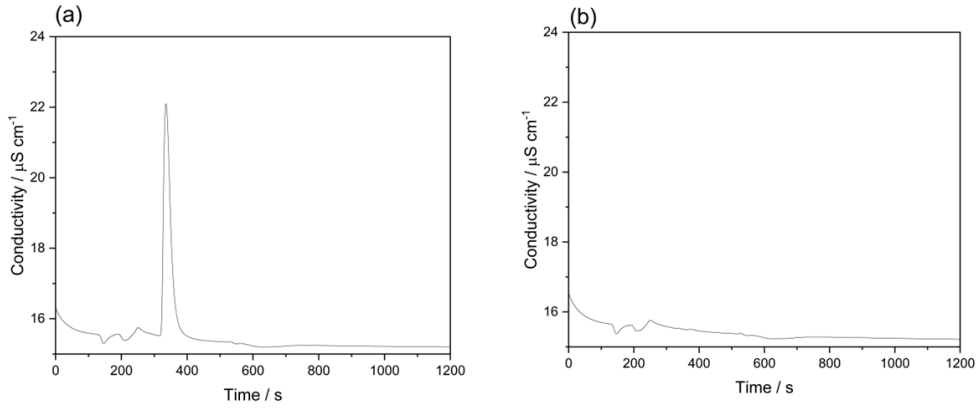

Figure S6. Ion chromatogram of $Pyr_{14}TFSI$ using an eluent 4 mM carbonate/sodium bicarbonate solution and a flow rate of 1 mL min^{-1} during 20 min. (a) without and (b) with water washing.

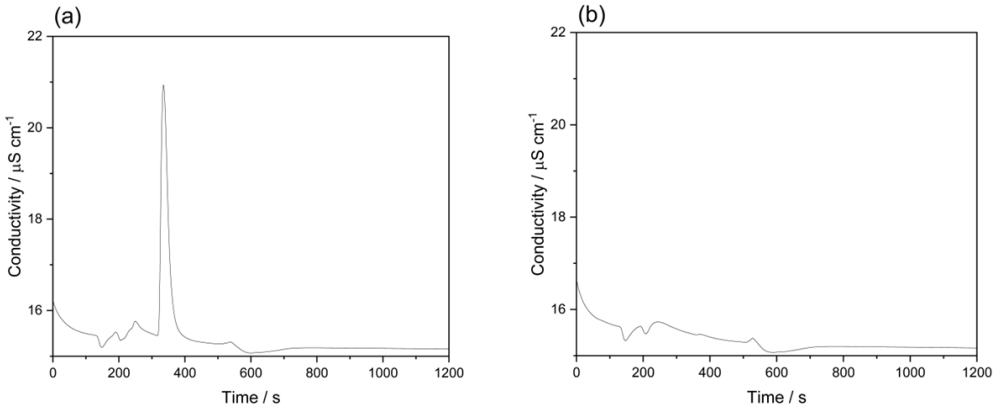

Figure S7. Ion chromatogram of $Pyr_{14}FSI$ using an eluent 4 mM carbonate/sodium bicarbonate solution and a flow rate of 1 mL min^{-1} during 20 min. (a) without and (b) with water washing.

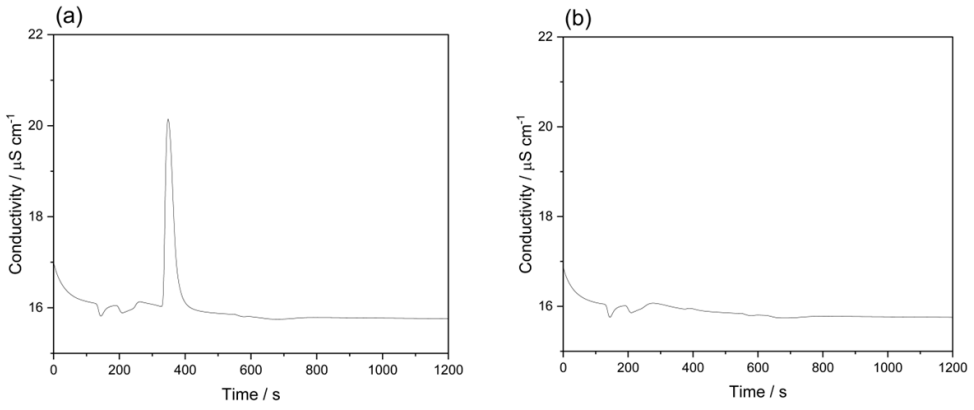

Figure S8. Ion chromatogram of $Pip_{14}TFSI$ using an eluent 4 mM carbonate/sodium bicarbonate solution and a flow rate of 1 mL min^{-1} during 20 min. (a) without and (b) with water washing.

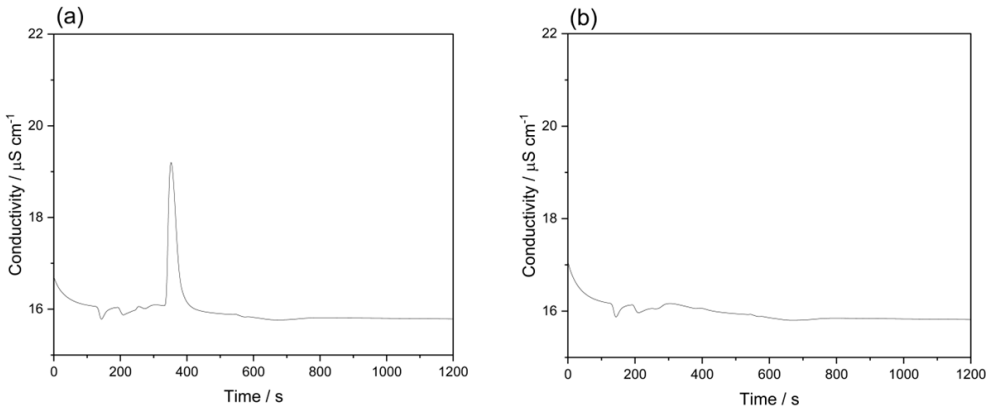

Figure S9. Ion chromatogram of BDMImTFSI using an eluent 4 mM carbonate/sodium bicarbonate solution and a flow rate of 1 mL min^{-1} during 20 min. (a) without and (b) with water washing.

Table S1. Impurities in commercial IL [12,13].

Ionic Liquids	$Br^{(a)}$ / ppm	$Na^{(b)}$ / ppm
$Pyr_{14}TFSI$	≤ 10-50*	≤ 50*
$Pyr_{14}FSI$	≤10-50*	≤ 50*
$Pyr_{14}TfO$	≤ 100**	≤ 3000**
Pip14TFSI	≤ 100**	-
BDMImTFSI	≤ 100**	-

Purity: *99.5 % and **99 %
(a)bromide+chloride+iodide and (b)potassium+lithium+sodium

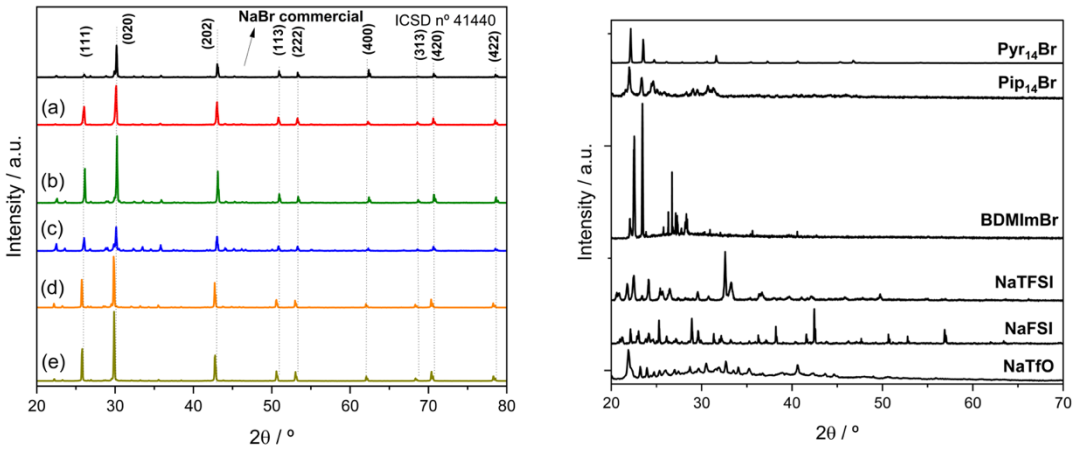

Figure S10. Left: PXRD pattern of the precipitate from the mechanochemical synthesis (500 rpm/ 240 min) of the following ILs: (a) $Pyr_{14}TFSI$, (b) $Pyr_{14}FSI$, (c) $Pyr_{14}TfO$, (d) $Pip_{14}TFSI$ and (e) BDMImTFSI. **Right**: PXRD pattern of the IL precursors.

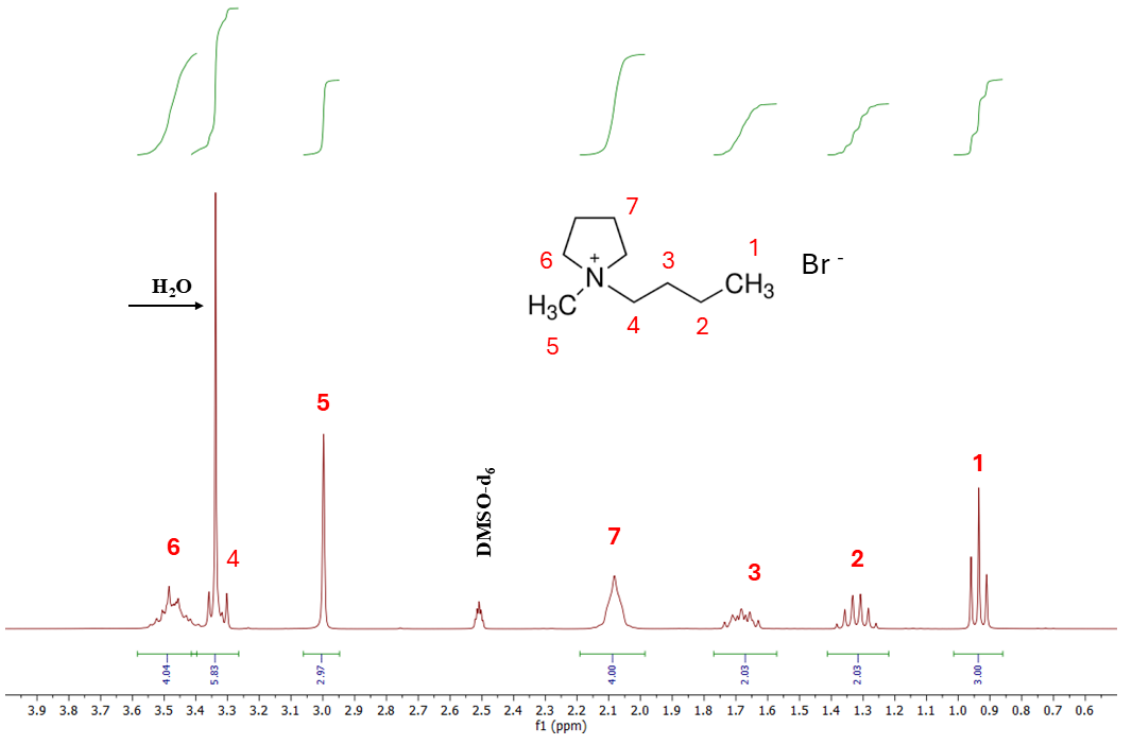

Figure S11. ^{1}H NMR spectrum of $Pyr_{14}Br$ at room temperature.

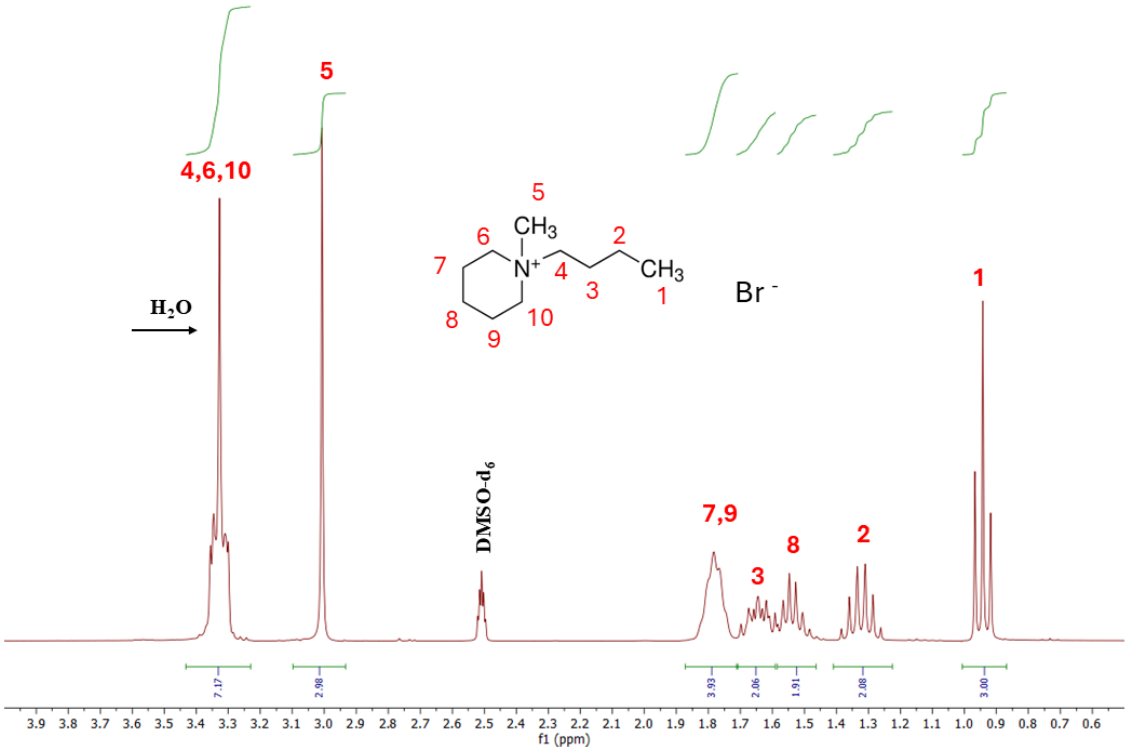

Figure S12. ^{1}H NMR spectrum of $Pip_{14}Br$ at room temperature.

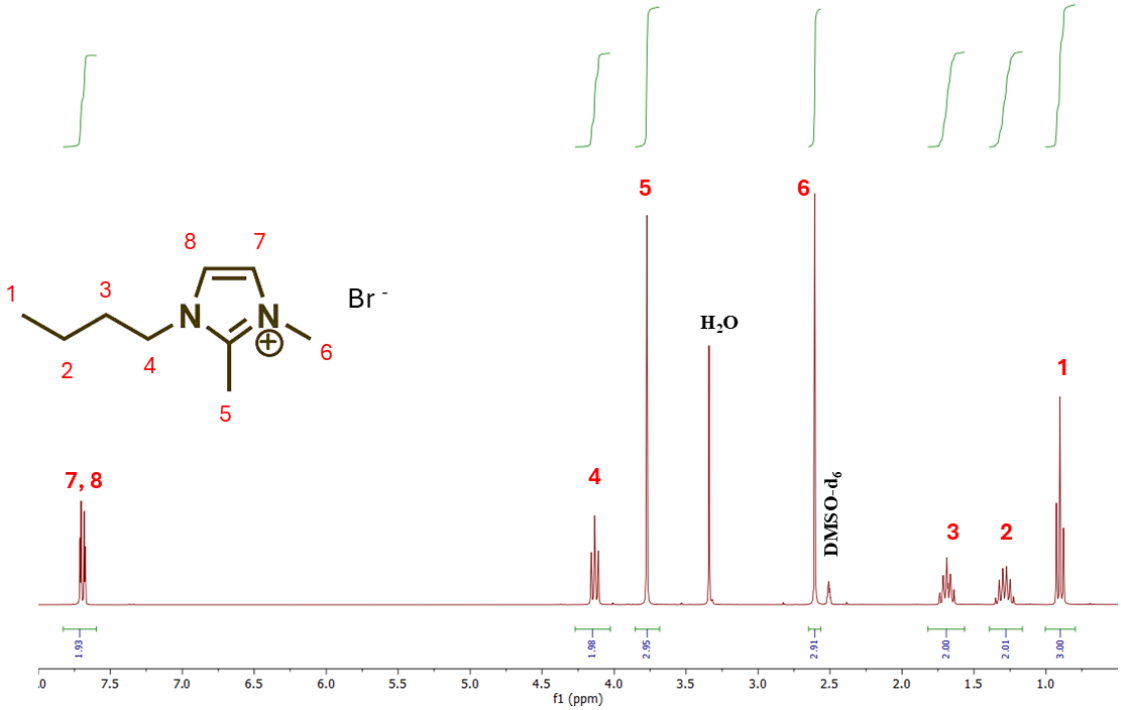

Figure S13. ^{1}H NMR spectrum of BDMImBr at room temperature.

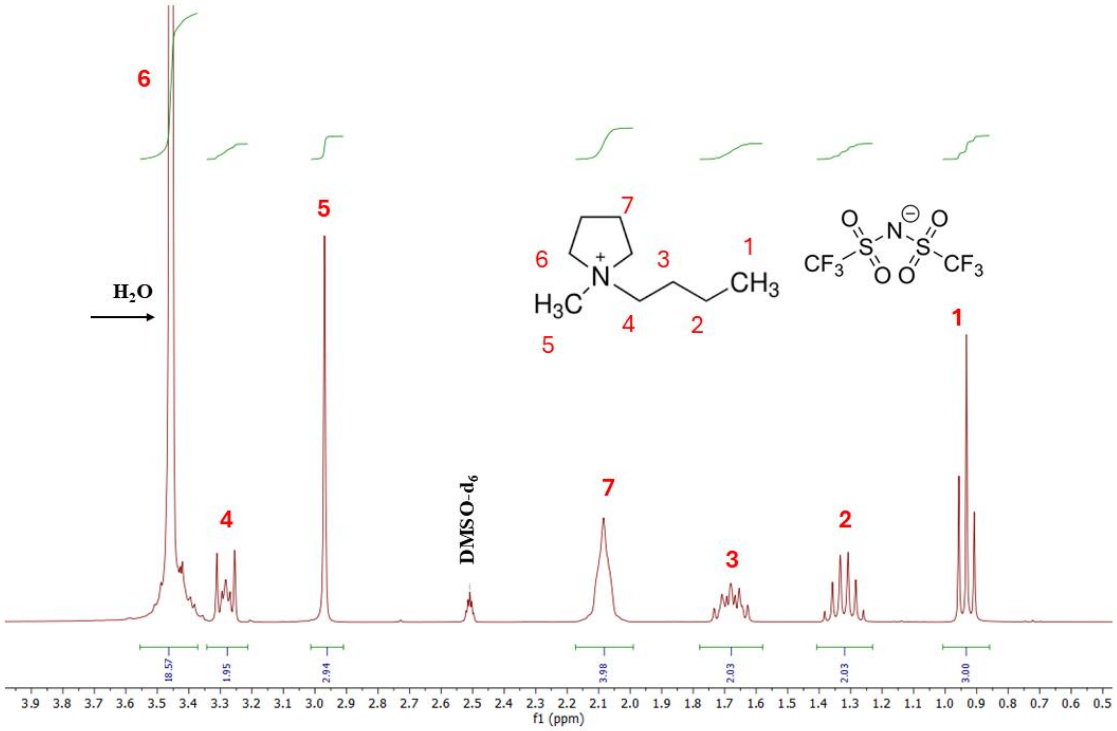

Figure S14. ^{1}H NMR spectrum of $Pyr_{14}TFSI$ at room temperature.

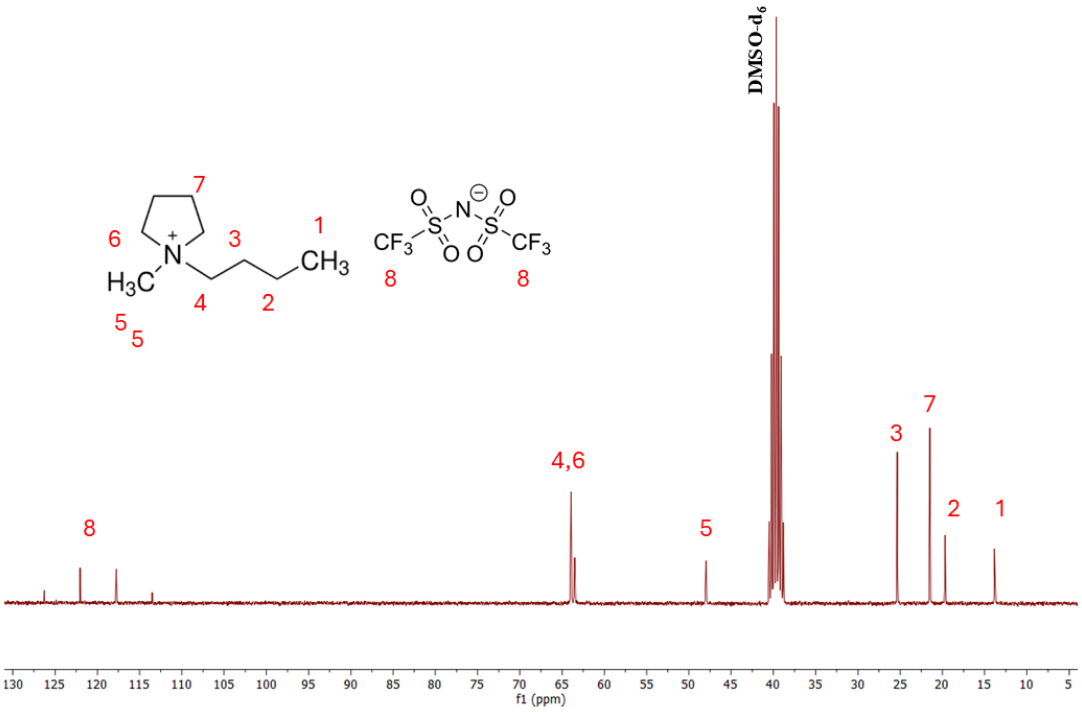

Figure S15. ^{13}C NMR spectrum of Pyr_{14}TFSI at room temperature.

Pyr_{14}TFSI data (300 MHz, DMSO-d^6; ppm) δ^1H: 3.43, 3.27 (m, 2H), 2.96 (s, 3H), 2.07 (m, 4H), 1.67 (m, 2H), 1.31 (h, J = 7.4 Hz, 2H), 0.92 (t, J = 7.3 Hz, 3H). δ^{13}C: 126.3, 122.1, 117.8, 113.5, 63.9, 63.5, 47.9, 25.4, 21.5, 19.7, 13.8.

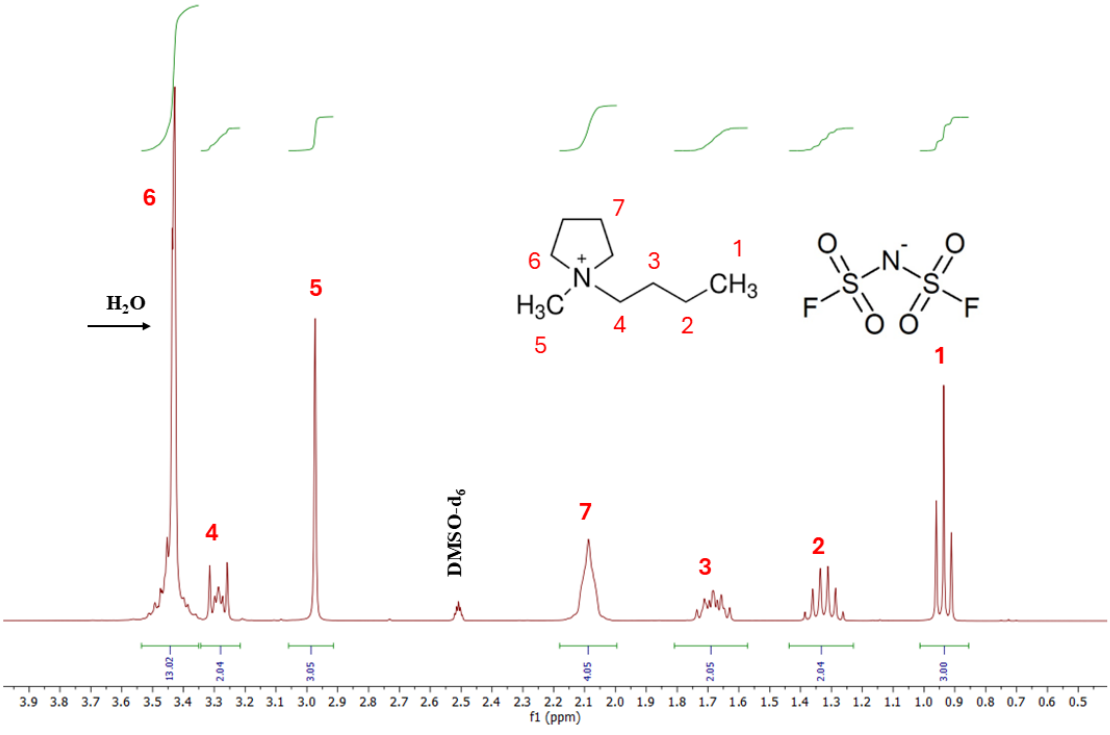

Figure S16. ^{1}H NMR spectrum of Pyr_{14}FSI at room temperature.

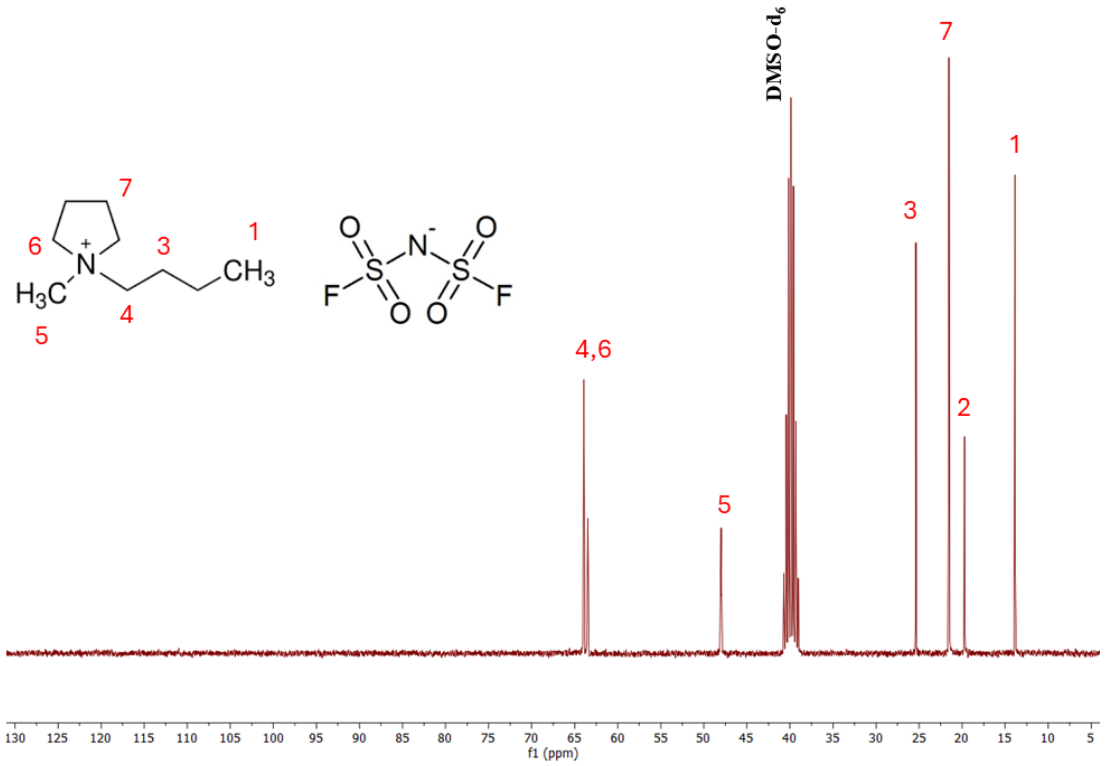

Figure S17. ^{13}C NMR spectrum of $Pyr_{14}FSI$ at room temperature.

$Pyr_{14}FSI$ data (300 MHz; DMSO-d^6; ppm) δ^1H: 3.42, 3.27 (m, 2H), 2.96 (s, 3H), 2.08 (m, 4H), 1.68 (m, 2H), 1.31 (h, J = 7.4 Hz, 2H), 0.93 (t, J = 7.3 Hz, 3H). δ^{13}C: 64.0, 63.5, 48.0, 25.4, 21.5, 19.7, 13.9.

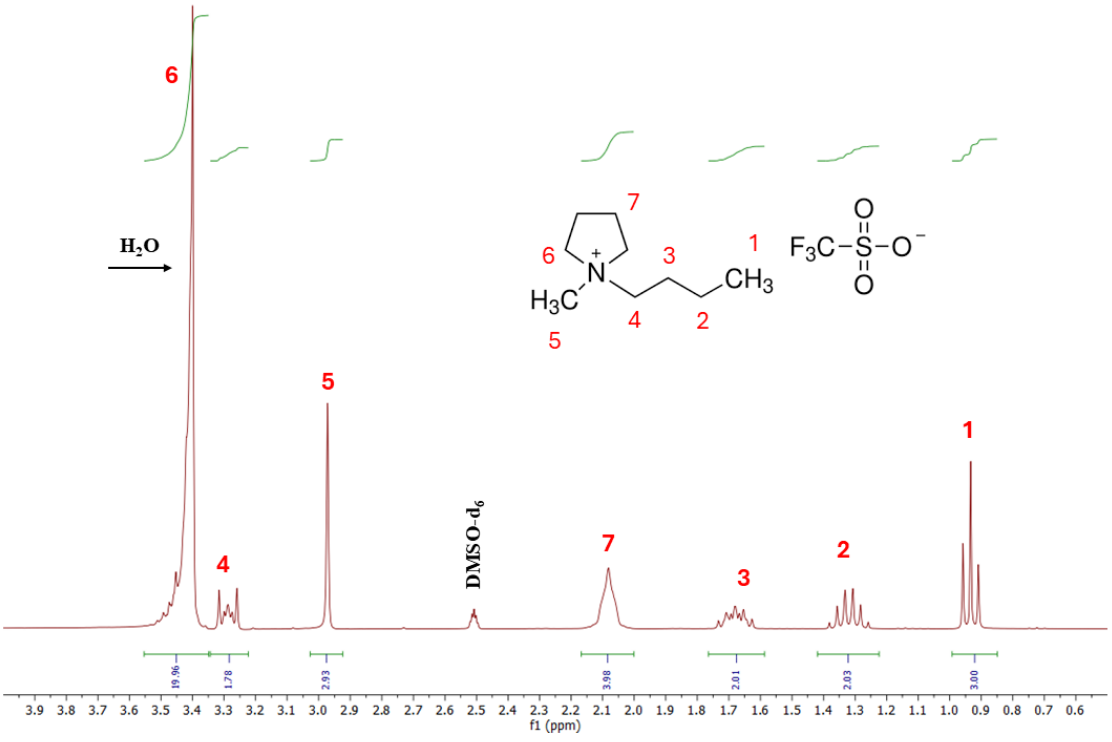

Figure S18. ^{1}H NMR spectrum of $Pyr_{14}TfO$ at room temperature.

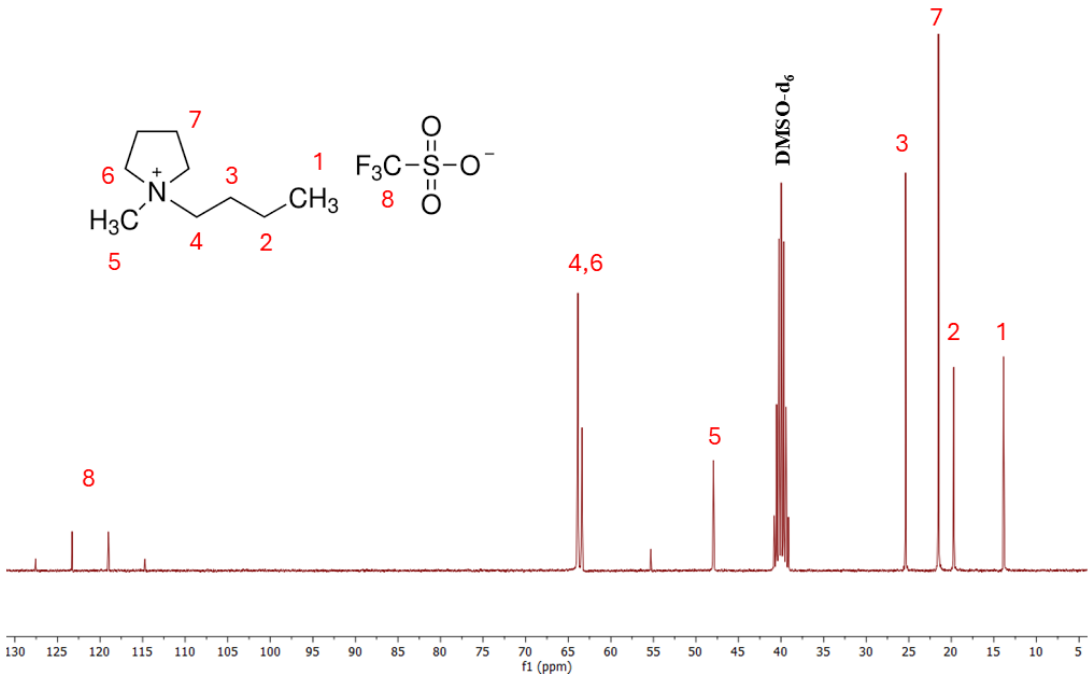

Figure S19. ^{13}C NMR spectrum of $Pyr_{14}TfO$ at room temperature.

$Pyr_{14}TfO$ data (300 MHz; DMSO-d^6; ppm). δ^1H: 3.44, 3.28 (m, 2H), 2.96 (s, 3H), 2.08 (q, J = 4.1 Hz, 4H), 1.67 (m, 2H), 1.31 (h, J = 7.4 Hz, 2H), 0.93 (t, J = 7.3 Hz, 3H). $\delta^{13}C$: 127.5, 123.3, 119.0, 114.8, 63.9, 63.4, 47.9, 25.4, 21.5, 19.7, 13.8.

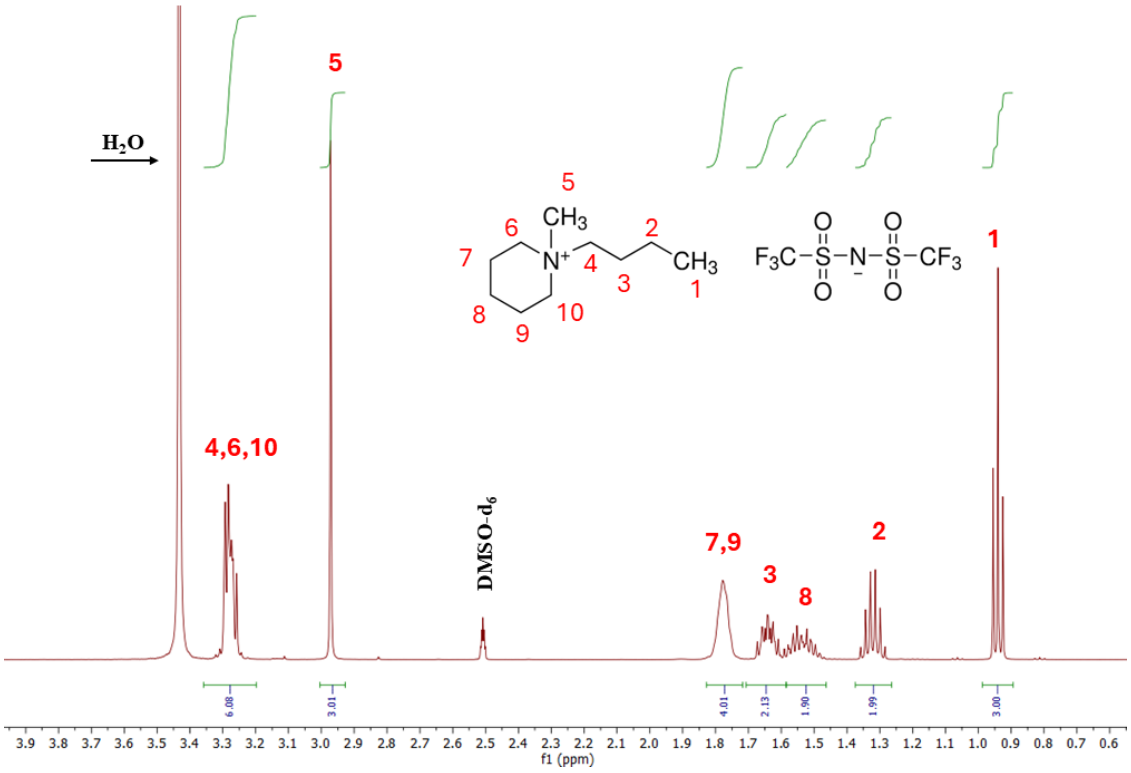

Figure S20. ^1H NMR spectrum of $Pip_{14}TFSI$ at room temperature.

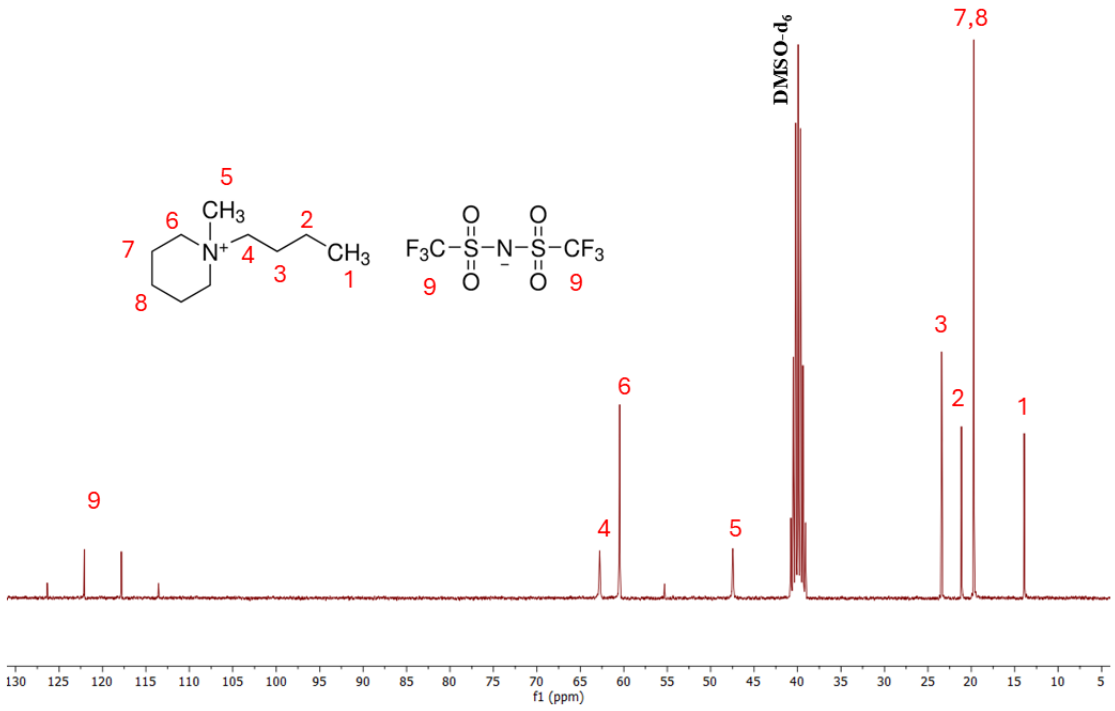

Figure S21. ^{13}C NMR spectrum of $Pip_{14}TFSI$ at room temperature.

$Pip_{14}TFSI$ data (300 MHz; DMSO-d^6; ppm). δ^1H: 3.36 – 3.19 (m, 6H), 2.96 (s, 3H), 1.84 – 1.69 (m, 4H), 1.69 – 1.45 (m, 4H), 1.31 (h, J = 7.4 Hz, 2H), 0.93 (t, J = 7.3 Hz, 3H). $\delta^{13}C$: 126.3, 122.1, 117.8, 113.6, 62.7, 60.5, 47.4, 23.4, 21.1, 19.7, 13.9.

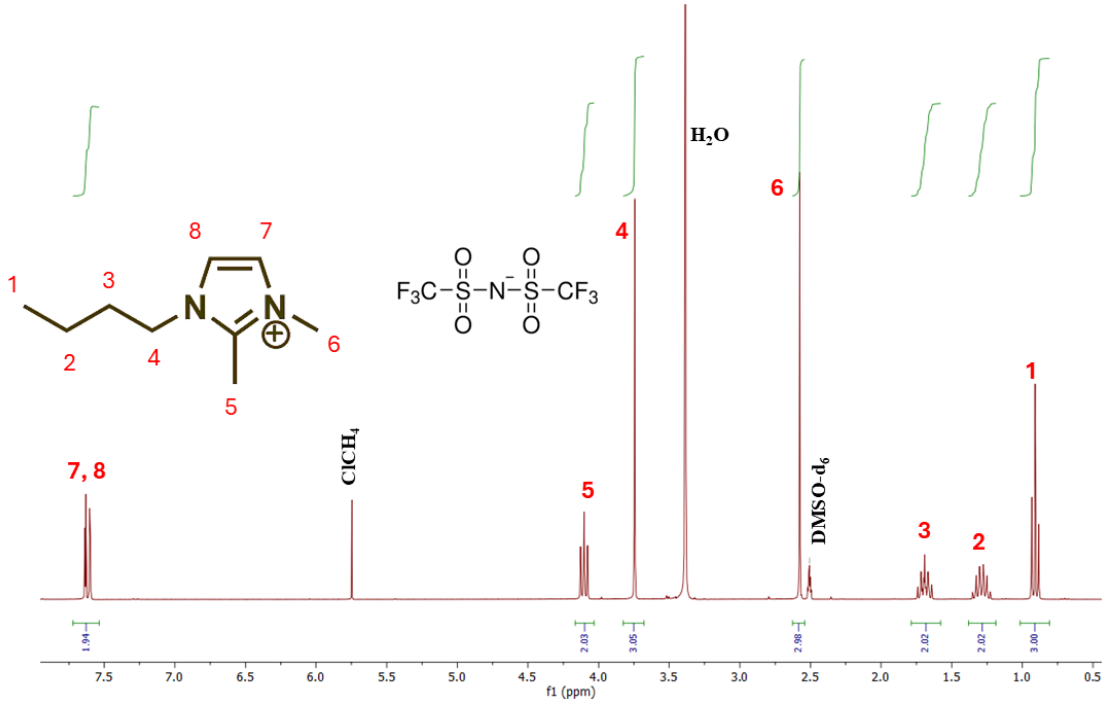

Figure S22. ^1H NMR spectrum of BDMImTFSI at room temperature.

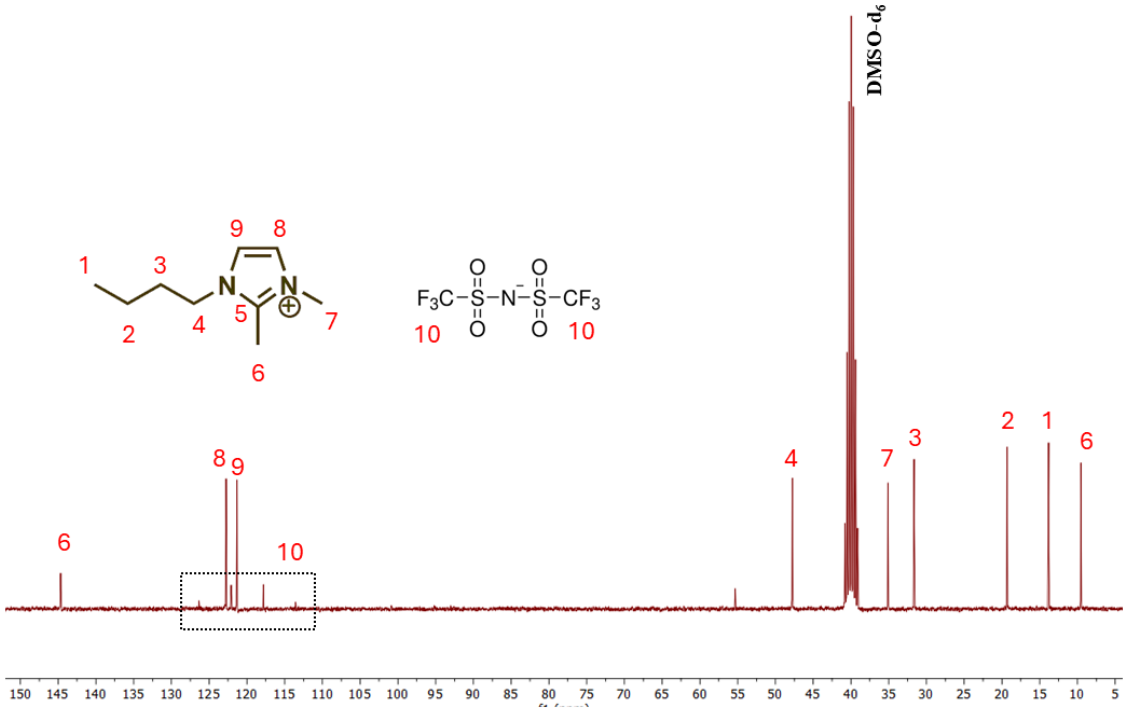

Figure S23. ^{13}C NMR spectrum of BDMImTFSI at room temperature.

BDMImTFSI data (300 MHz; DMSO-d^6; ppm). δ^1H: 7.61 (m, 2H), 4.10 (t, J = 7.3 Hz, 2H), 3.74 (s, 3H), 2.57 (s, 3H), 1.68 (m, 2H), 1.28 (m, 2H), 0.90 (t, J = 7.3 Hz, 3H). $\delta^{13}C$: 144.7, 126.3, 122.8, 122.1, 121.3, 117.8, 113.5, 47.8, 40.8, 35.1, 31.6, 19.3, 13.8, 9.5.

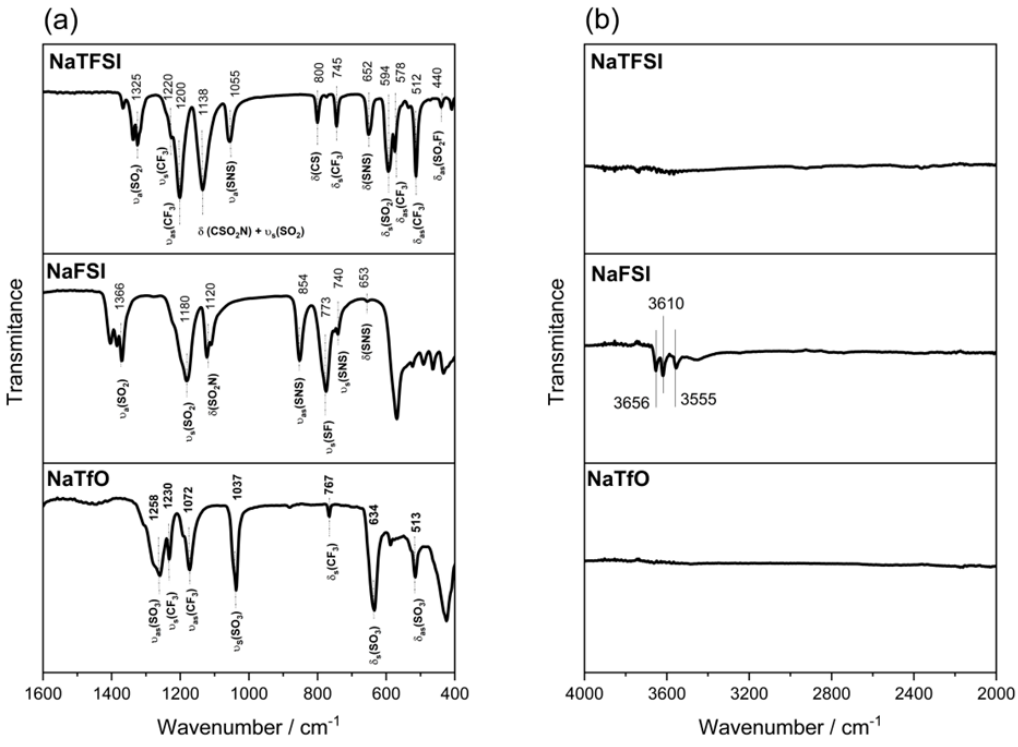

Figure S24. FTIR Spectra of the precursor salts: (a) range 400 – 1600 cm^{-1}, and (b) 2000 – 4000 cm^{-1}.

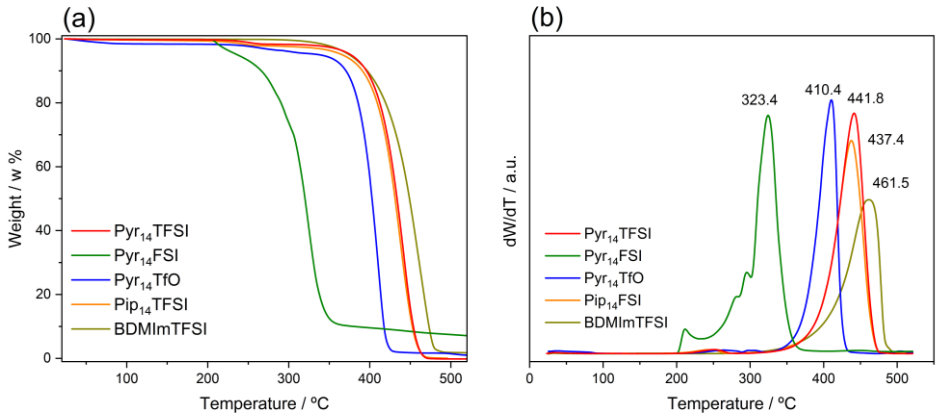

Figure S25. TGA (a) and differential (b) curves of ILs synthesized by mechanochemical route. Scan rate: 10 ºC min^{-1}.

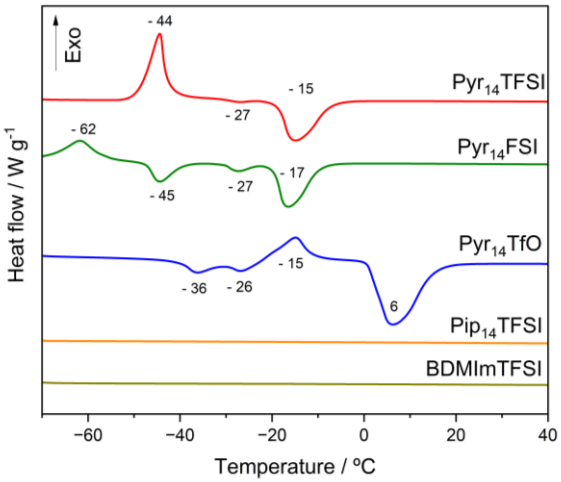

Figure S26. DSC curves of ILs synthesized by mechanochemical route. Scan rate: 10 ºC min^{-1}.

Table S2. Experimental Values of Ionic Conductivity (σ), Viscosity (η) and Density (ρ) of $Pyr_{14}TFSI$ at Several Temperatures and at atmospheric pressure. Standard uncertainties are u(σ) = 0.05σ, u (η) = 0.002, u(ρ) = 0.0003 g cm^{-3} and u(T) = 0.01 K.

T / K	T / ºC	Conductivity / $mScm^{-1}$	Viscosity / mPa s	Density/ g cm^{-3}
298.15	25	3.90	77.82	1.394
300.15	27	4.22	71.03	1.392
306.15	33	5.22	54.86	1.387
312.15	39	6.40	43.28	1.381
318.15	45	7.82	34.79	1.376
324.15	51	9.26	28.43	1.371
330.15	57	10.83	23.58	1.366
336.15	63	12.60	19.82	1.361
341.15	68	14.02	17.31	1.356
348.15	75	16.10	14.49	1.350

Table S3. Experimental Values of Ionic Conductivity (σ), Viscosity (η) and Density (ρ) of $Pyr_{14}FSI$ at Several Temperatures and at atmospheric pressure. Standard uncertainties are u(σ) = 0.05σ, u (η) = 0.002, u(ρ) = 0.0003 g cm^{-3} and u(T) = 0.01 K.

T / K	T / ºC	Conductivity / mS cm^{-1}	Viscosity / mPa s	Density/ g cm^{-3}
298.15	25	8.59	53.68	1.306
300.15	27	9.04	50.03	1.305
306.15	33	10.66	40.93	1.300
312.15	39	12.48	33.95	1.295
318.15	45	14.45	28.51	1.291
324.15	51	16.41	24.21	1.286
330.15	57	18.40	20.78	1.282
336.15	63	20.51	17.99	1.277
341.15	68	22.26	16.05	1.274
348.15	75	24.69	13.81	1.268

Table S4. Experimental Values of Ionic Conductivity (σ), Viscosity (η) and Density (ρ) of $Pyr_{14}TfO$ at Several Temperatures and at atmospheric pressure. Standard uncertainties are u(σ) = 0.05σ, u (η) = 0.002, u(ρ) = 0.0003 g cm^{-3} and u(T) = 0.01 K.

T / K	T / ºC	Conductivity / mS cm^{-1}	Viscosity / mPa s	Density/ g cm^{-3}
298.15	25	2.69	176.65	1.252
300.15	27	2.91	159.05	1.250
306.15	33	3.69	117.67	1.246
312.15	39	4.66	89.20	1.242
318.15	45	5.87	69.09	1.237
324.15	51	7.24	54.57	1.233
330.15	57	8.63	43.83	1.229
336.15	63	10.35	35.76	1.225
341.15	68	11.80	30.50	1.221
348.15	75	14.03	24.77	1.216

Table S5. Experimental Values of Ionic Conductivity (σ), Viscosity (η) and Density (ρ) of $Pip_{14}TFSI$ at Several Temperatures and at atmospheric pressure. Standard uncertainties are u(σ) = 0.05σ, u (η) = 0.002, u(ρ) = 0.0003 g cm^{-3} and u(T) = 0.01 K.

T / K	T / ºC	Conductivity / mS cm^{-1}	Viscosity / mPa s	Density/ g cm^{-3}
298.15	25	1.61	184.38	1.378
300.15	27	1.78	163.88	1.377
306.15	33	2.39	117.52	1.371
312.15	39	3.13	86.78	1.366
318.15	45	3.92	65.77	1.361
324.15	51	4.79	51.01	1.356
330.15	57	5.79	40.37	1.351
336.15	63	6.94	32.54	1.346
341.15	68	7.92	27.53	1.342
348.15	75	9.44	22.14	1.336

Table S6. Experimental Values of Ionic Conductivity (σ), Viscosity (η) and Density (ρ) of BDMImTFSI at Several Temperatures and at atmospheric pressure. Standard uncertainties are u(σ) = 0.05σ, u (η) = 0.002, u(ρ) = 0.0003 g cm^{-3} and u(T) = 0.01 K.

T / K	T / ºC	Conductivity / mS cm^{-1}	Viscosity / mPa s	Density/ g cm^{-3}
298.15	25	3.15	100.36	1.418
300.15	27	3.45	90.59	1.416
306.15	33	4.46	67.87	1.411
312.15	39	5.65	52.12	1.405
318.15	45	6.88	40.91	1.400
324.15	51	8.22	32.74	1.394
330.15	57	9.95	26.65	1.389
336.15	63	11.30	22.03	1.383
341.15	68	12.64	18.20	1.379
348.15	75	14.49	15.66	1.373

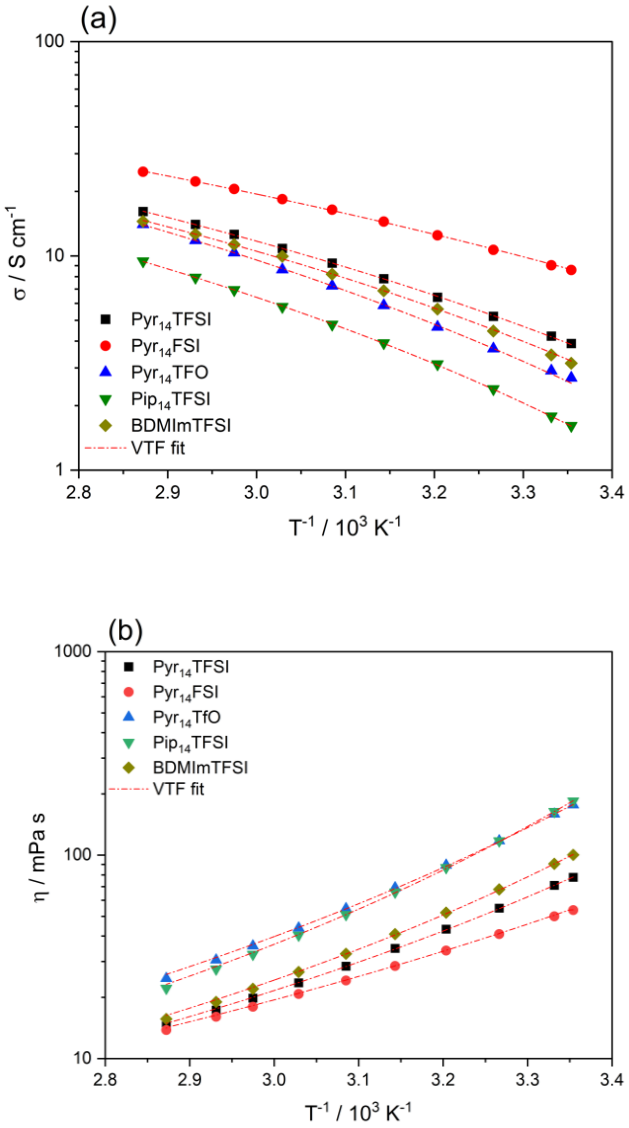

Figure S27. Conductivity (a), viscosity (b) vs. temperature of ILs synthesized using a ball mill.

Table S7. VTF fit parameters for conductivity.

Ionic Liquid	σ_o	B	T_o	B/T_o
$Pyr_{14}TFSI$	0.377 ± 0.006	- 503.9 ± 2.3	188.15	2.7
$Pyr_{14}FSI$	0.380 ± 0.008	- 488.4 ± 3.3	169.15	2.9
$Pyr_{14}TfO$	0.518 ± 0.017	- 564.2 ± 4.6	192.00	2.9
$Pip_{14}TFSI$	0.298 ± 0.004	- 510.1 ± 1.9	200.05	2.5
BDMImTFSI	0.301 ± 0.011	- 453.8 ± 5.2	198.05	2.3

Table S8. VTF fit parameters for viscosity.

Ionic Liquid	η_o	B	T_o
$Pyr_{14}TFSI$	0.39 ± 0.01	583.4 ± 2.9	188.15
$Pyr_{14}FSI$	0.44 ± 0.01	618.8 ± 3.3	169.15
$Pyr_{14}TfO$	0.44± 0.02	638.0 ± 4.1	192.00
$Pip_{14}TFSI$	0.39 ± 0.01	604.0 ± 3.5	200.15
BDMImTFSI	0.42 ± 0.01	547.6 ± 3.4	198.15

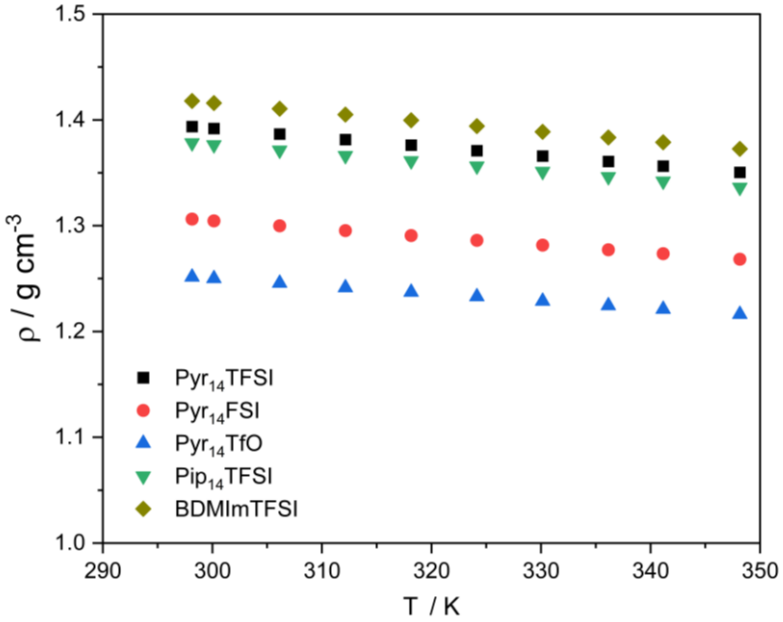

Figure S28. Density vs. temperature dependence of ILs synthesized.

Table S9. Experimental and calculated densities at 298 K.

ILs	r_{calc} / g cm^{-3}	r_{exp} / g cm^{-3}	| Error | / %
$Pyr_{14}TFSI$	1.400	1.394	0.5
$Pyr_{14}FSI$	1.366	1.306	4.4
$Pyr_{14}TfO$	1.266	1.252	1.2
$Pip_{14}TFSI$	1.396	1.378	1.3
BDMImTFSI	1.389	1.418	2.1

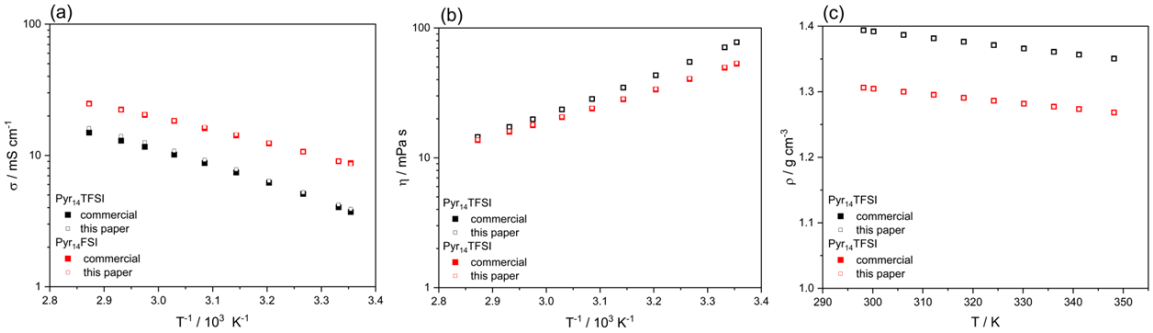

Figure S29. Ionic conductivity (a). viscosity (b). and density(c) of the ILs $Pyr_{14}TFSI$ and $Pyr_{14}FSI$ and their commercial analogues.

Table S10. Physicochemical and electrochemical properties of ILs by other synthesis methods.

Ionic Liquid	σ / mS cm-1	η / mPa s	d / g cm-3	EW / V	Ref.
$Pyr_{14}TFSI$	3.9 – 4.0 (25 ºC) 16.4 – 17.2 (75 ºC)	72.6 – 77.76 (25 ºC) 12.0 – 14.5 (75 ºC)	1.395 – 1.442 (25 ºC) 1.350 – 1.366 (75 ºC)	5.2 – 6.0	[3].[14].[15].[16].[17].[18].[19].[20].[21]
$Pyr_{14}FSI$	6.2 – 8.7 (25ºC) 20.7 – 26.9 (75ºC)	53.2 (25 ºC) 13.7 – 13.8 (75 ºC)	1.307 (25 ºC) 1.267 (75 ºC)	5.1	[3].[22].[23]
$Pyr_{14}TfO$	1.3 (20 ºC) - 20.0 (80 ºC)	158 (20 ºC) - -	1.256 (20 ºC) 1.252 (25 ºC) 1.210 (80 ºC)	5.0	[4].[24]
$Pip_{14}TFSI$	1.2 – 1.4 (25 ºC) 8.8 (75 ºC)	153 – 189 (25 ºC) 22.0 - 22.5 (75 ºC)	1.382 (25 ºC) 1.339 (75 ºC)	4.5 – 5.1	[3].[25].[26].[27]
BDMImTFSI	2.4 (25 ºC) 11.8 (70 ºC)	134.2 (25 ºC) 15.8 (75 ºC)	1.424 (25 ºC) 1.379 (75 ºC)	4.5	[28].[29].[30].[31]

Table S11. Physicochemical and electrochemical properties of commercial ILs [12,13].

Ionic Liquids	σ / mS cm^{-1}	η / mPa s	d / g cm^{-3}	EW / V
$Pyr_{14}TFSI$	2.120 (20 ºC)	94.0 (20 ºC)	1.400 (23 ºC)	5.3
$Pyr_{14}FSI$	4.357 (25ºC)	52.0 (25 ºC)	1.304 (25 ºC)	-
$Pyr_{14}TfO$	1.850 (24 ºC)	148.0 (25 ºC)	1.250 (27 ºC)	4.2
$Pip_{14}TFSI$	0.835 (25 ºC)	183.2 (20 ºC)	1.382 (23 ºC)	3.7
BDMImTFSI	1.958 (25 ºC)	98.0 (25 ºC)	1.420 (25 ºC)	4.6

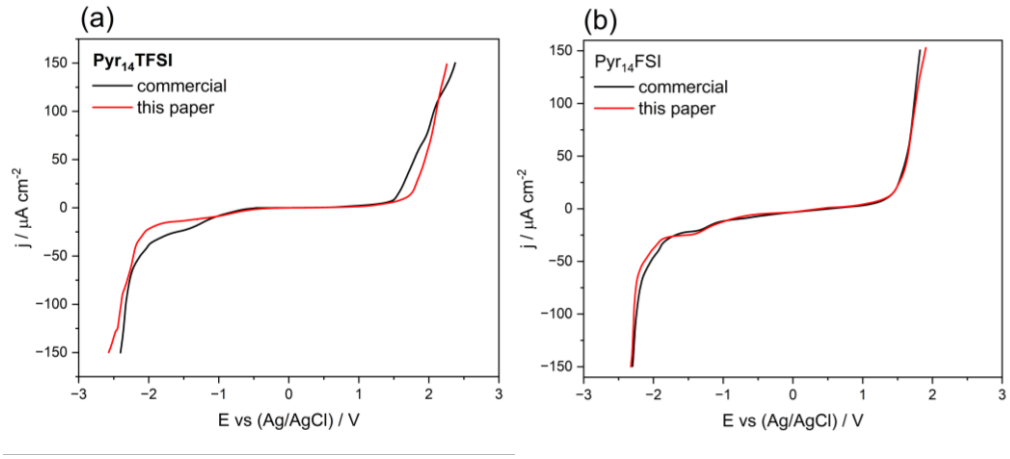

Figure S30. Linear sweep voltammetry of Pyr14TFSI (a) and Pyr14FSI (b) and synthesized by mechanochemical and commercial. Aluminum/carbon as the work electrode and active carbon as counter electrode. The reference electrode is an Ag/AgCl wire. Scan rate: 5 mV s-1.

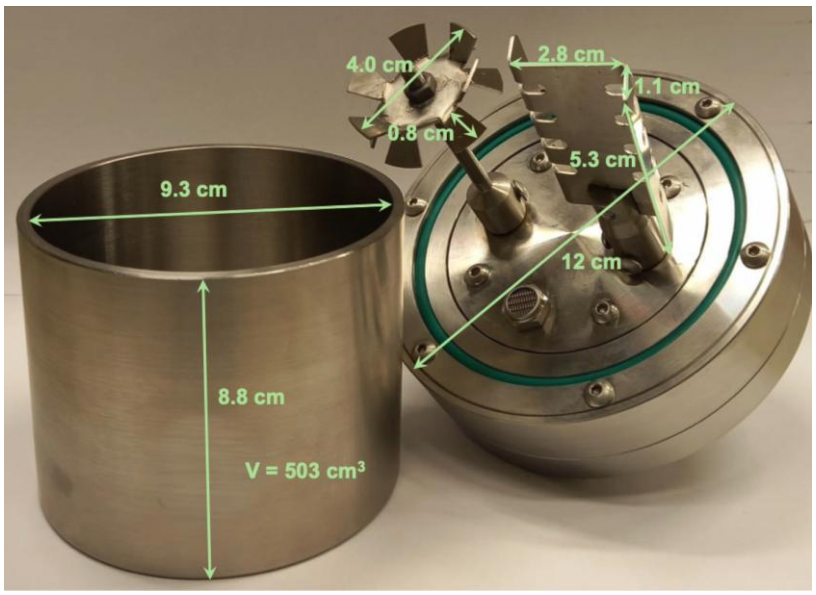

Figure S31 - Vessel and paddles used in the synthesis of $Pyr_{14}TFSI$ in scale up. The vessel is a stainless-steel cylindrical mixing chamber equipped with a multi-shaft stirring system mounted on the lid. The lid contains two independent stirring shafts, each fitted with different impeller geometries designed to handle high-viscosity, solid–liquid, or semi-solid mixtures. One shaft carries a paddle impeller, while the second carries a multi-blade dispersing impeller with serrated edges, enabling simultaneous shear generation, bulk mixing, and scraping-like flow patterns.

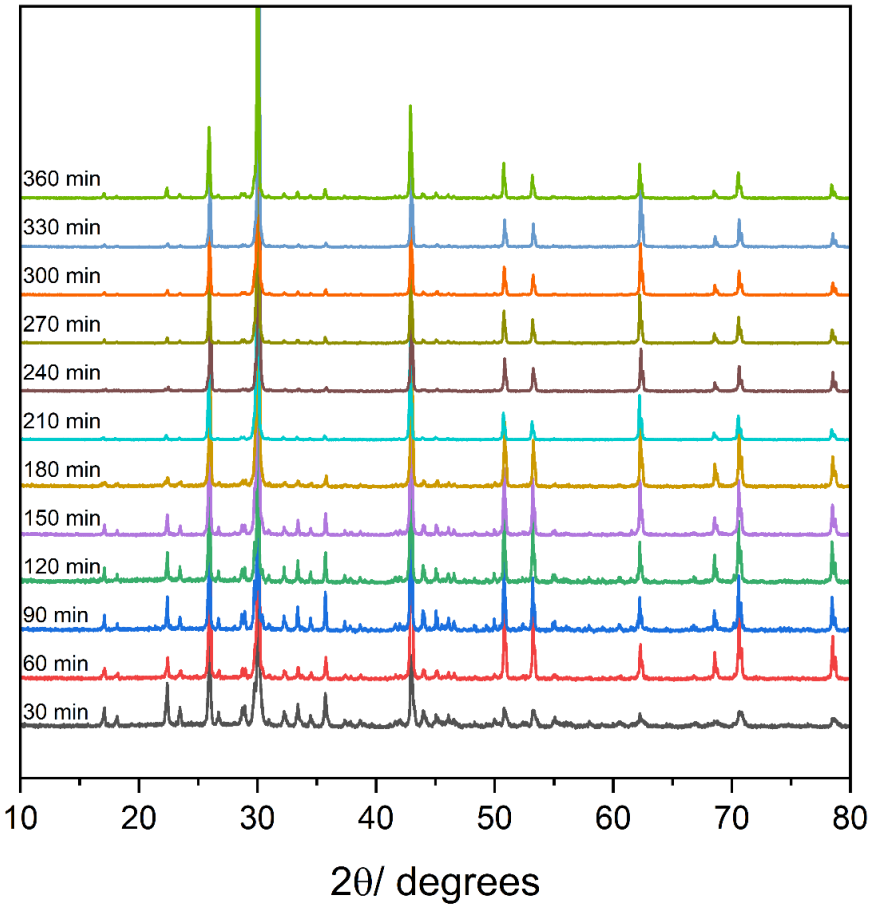

Figure S32. XRD pattern of NaBr obtained from the scale-up synthesis of $Pyr_{14}TFSI$.

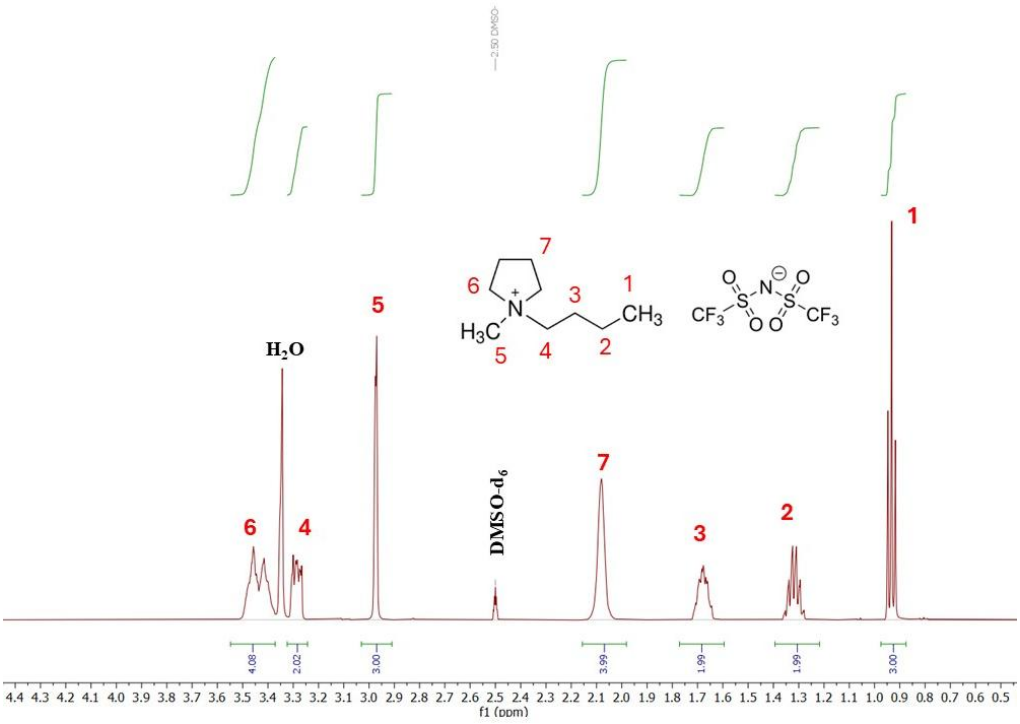

Figure S33. ^{1}H NMR spectrum of $Pyr_{14}TFSI$ obtained after scale-up following 30 minutes of reaction.

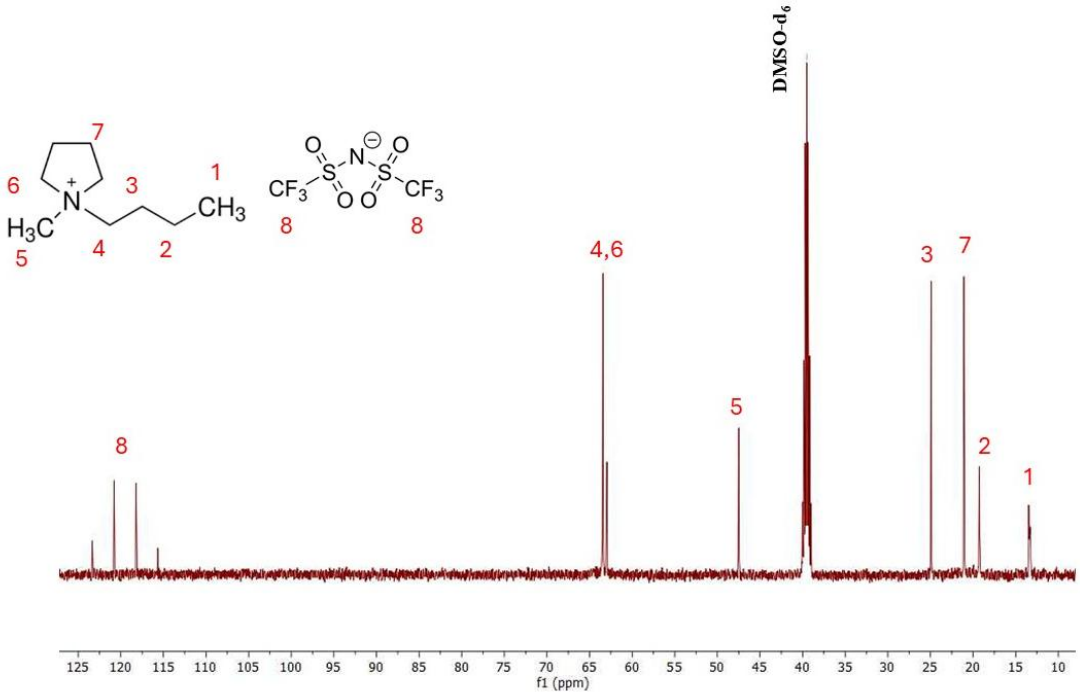

Figure S34. ^{13}C NMR spectrum of $Pyr_{14}TFSI$ obtained after scale-up following 360 minutes of reaction.

$Pyr_{14}TFSI$ data (300 MHz. DMSO-d^6; ppm) δ^1H: 3.43. 3.27 (m. 2H). 2.96 (s. 3H). 2.07 (m. 4H). 1.67 (m. 2H). 1.31 (h. J = 7.4 Hz. 2H). 0.92 (t. J = 7.3 Hz. 3H). $\delta^{13}C$: 126.3. 122.1. 117.8. 113.5. 63.9. 63.5. 47.9. 25.4. 21.5. 19.7. 13.8.

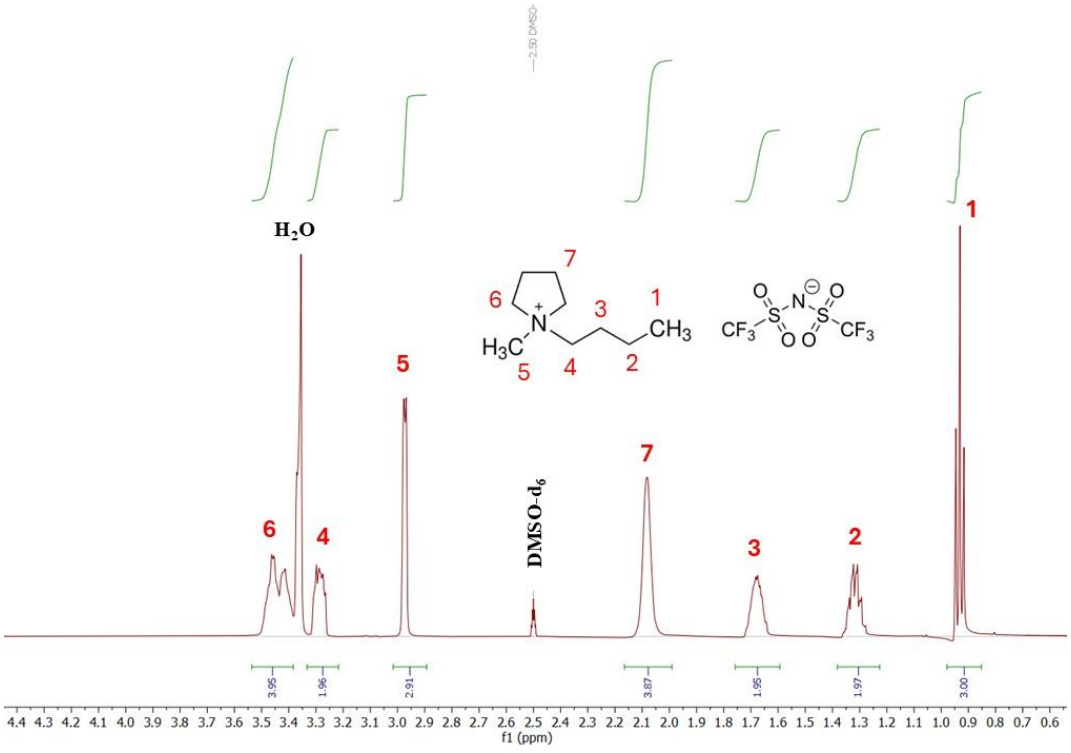

Figure S35. ^1H NMR spectrum of $Pyr_{14}TFSI$ obtained after scale-up following 360 minutes of reaction.

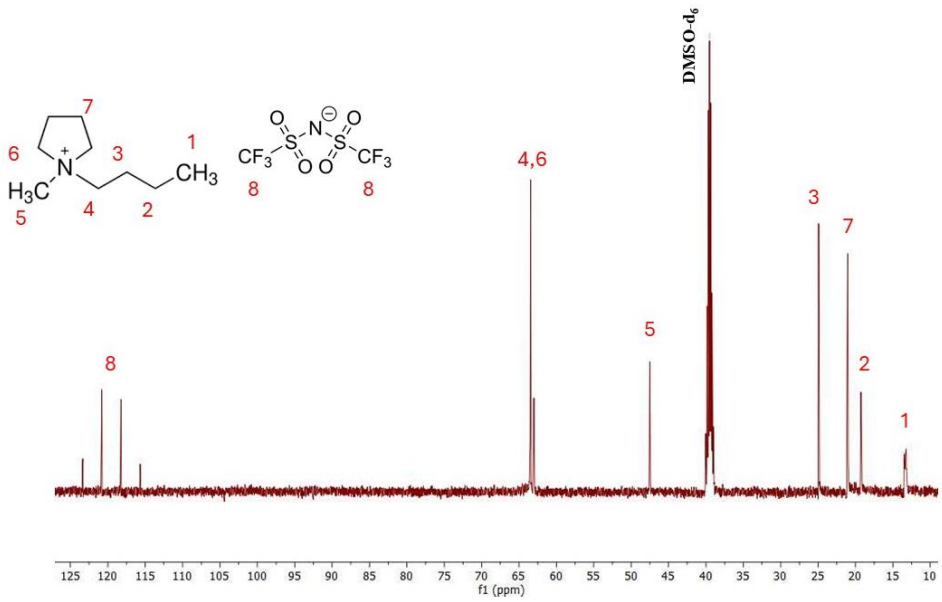

Figure S36. ^{13}C NMR spectrum of $Pyr_{14}TFSI$ obtained after scale-up following 360 minutes of reaction.

$Pyr_{14}TFSI$ data (300 MHz. DMSO-d^6; ppm) δ^1H: 3.43. 3.27 (m. 2H). 2.96 (s. 3H). 2.07 (m. 4H). 1.67 (m. 2H). 1.31 (h. J = 7.4 Hz. 2H). 0.92 (t. J = 7.3 Hz. 3H). $\delta^{13}C$: 126.3. 122.1. 117.8. 113.5. 63.9. 63.5. 47.9. 25.4. 21.5. 19.7. 13.8.

Table S12. Amount of Br in $Pyr_{14}TFSI$ prepared by planetary mixing at 100 g scale.

Reaction time / min	Removed mass / g	Br / ppm
30	0.26	26.79
60	0.50	42.47
90	0.30	40.83
120	0.47	42.85
150	1.09	44.48
180	0.57	36.20
210	0.59	39.60
240	0.79	38.18
270	0.58	43.11
300	0.90	40.42
330	0.89	41.91
360	1.09	41.16
360*	-	38.23

* IL washing with deionized water.

Table S13. Comparative parameters between the ball mill (lab scale) and the mixer (scale-up) approaches for $Pyr_{14}TFSI$ synthesis.

Parameters	Ball mill	Mixer
Reagents / g	4.7	99.3
Solvent/mL $g_{product}^{-1}$	5.5	0.6
Water/ mL $g_{product}^{-1}$	55.6	2.4
Conversion / % (Time-to-convertion / min)	> 99 (240 min)	> 99 (360 min) 97 (30 min)
Yield* / %	89.4*	88.4*
Br^+ / ppm	17.9*	38.2 * (360 min) 26.8 ** (30 min) 41.2 ** (360 min)
Na^+ / ppm	< 0.01*	< 0.01* (360 min)
E-factor	7.7	1.0
cE-factor	63.4*	3.4* 0.2**

Conditions: *filtration + washing; ** only centrifugation.

References

1 C. Villagrán, M. Deetlefs, W. R. Pitner and C. Hardacre, *Anal. Chem.*, 2004, **76**, 2118–2123.

2 F. Hao, P. R. Haddad and T. Ruther, *Chromatographia*, 2008, **67**, 495–498.

3 N. Sánchez-Ramírez, B. D. Assresahegn, D. Bélanger and R. M. Torresi, *J. Chem. Eng. Data*, 2017, **62**, 3437–3444.

4 M. Moreno, M. Montanino, M. Carewska, G. B. Appetecchi, S. Jeremias and S. Passerini, *Electrochim. Acta*, 2013, **99**, 108–116.

5 V. L. Martins, N. Sanchez-Ramirez, M. C. C. Ribeiro and R. M. Torresi, *Phys. Chem. Chem. Phys.*, 2015, **17**, 23041–23051.

6 M. Kunze, S. Jeong, E. Paillard, M. Winter and S. Passerini, *J. Phys. Chem. C*, 2010, **114**, 12364–12369.

7 A. V. Agafonov, L. M. Ramenskaya, E. P. Grishina and N. O. Kudryakova, *RSC Adv.*, 2021, **11**, 38605–38615.

8 O. V. Alekseeva, V. D. Shibaeva, A. V. Noskov and A. V. Agafonov, *J. Mol. Liq.*, 2024, **405**, 125086.

9 C. Ye and J. M. Shreeve, *J. Phys. Chem. A*, 2007, **111**, 1456–1461.

10 G. Laus, G. Bentivoglio, V. Kahlenberg, K. Wurst, G. Nauer, H. Schottenberger, M. Tanaka and H.-U. Siehl, *Cryst. Growth Des.*, 2012, **12**, 1838–1846.

11 V. Chaudoy, J. Jacquemin, F. Tran-Van, M. Deschamps and F. Ghamouss, *Pure Appl. Chem.*, 2019, **91**, 1361–1381.

12 Solvionic, catalog products, available at: https://solvionic.com/en/10-products , accessed November 2025.

13 Ionic Liquids Technologies, catalog products, available at: https://iolitec.de/products/ionic_liquids/catalogue , accessed November 2025.

14 M. Vranes, S. Dozic, V. Djeric and S. Gadzuric, *J. Chem. Eng. Data*, 2012, **57**, 1072–1077.

15 M. Krummen, P. Wasserscheid and J. Gmehling, *J. Chem. Eng. Data*, 2002, **47**, 1411–1417.

16 M. Shamsipur, A. A. M. Beigi, M. Teymouri, S. M. Pourmortazavi and M. Irandoust, *J. Mol. Liq.*, 2010, **157**, 43–50.

17 R. Kato and J. Gmehling, *J. Chem. Thermodyn.*, 2005, **37**, 603–619.

18 R. Zarrougui, M. Dhahbi and D. Lemordan, *J. Electroanal. Chem.*, 2014, **717–718**, 189–195.

19 A. M. O'Mahony, D. S. Silvester, L. Aldous, C. Hardacre and R. G. Compton, *J. Chem. Eng. Data*, 2008, **53**, 2884–2891.

20 G. B. Appetecchi, M. Montanino, A. Balducci, S. F. Lux, M. Winter and S. Passerini, *J. Power Sources*, 2009, **192**, 599–605.

21 A. R. Neale, C. Schütter, P. Wilde, P. Goodrich, C. Hardacre, S. Passerini, A. Balducci and J. Jacquemin, *J. Chem. Eng. Data*, 2017, **62**, 376–390.

22 T. Makino, M. Kanakubo, T. Umecky, A. Suzuki, T. Nishida and J. Takano, *J. Chem. Eng. Data*, 2012, **57**, 751–755.

23 Q. Zhou, W. A. Henderson, G. B. Appetecchi, M. Montanino and S. Passerini, *J. Phys. Chem. B*, 2008, **112**, 13577–13580.

24 E. Vercher, V. González-Alfaro, F. J. Llopis, A. V. Orchillés, P. J. Miguel and A. Martínez-Andreu, *J. Chem. Thermodyn.*, 2018, **118**, 292–301.

25 M. Montanino, M. Carewska, F. Alessandrini, S. Passerini and G. B. Appetecchi, *Electrochim. Acta*, 2011, **57**, 153–159.

26 F. F. C. Bazito, Y. Kawano and R. M. Torresi, *Electrochim. Acta*, 2007, **52**, 6427–6437.

27 A. Bhattacharjee, P. J. Carvalho and J. A. P. Coutinho, *Fluid Phase Equilib.*, 2014, **375**, 80–88.

28 H. Zhang, X. Cui, P. Li, T. Feng and H. Feng, *J. Mol. Liq.*, 2022, **365**, 120193.

29 F. M. Gaciño, T. Regueira, L. Lugo, M. J. P. Comuñas and J. Fernández, *J. Chem. Eng. Data*, 2011, **56**, 4984–4999.

30 P. Schmitz, M. Kolek, M. Pyschik, K. Jalkanen, S. Nowak, M. Winter and P. Bieker, *ChemistrySelect*, 2017, **2**, 6052–6056.

31 C. Yan, L. Zaijun, Z. Hailang, F. Yinjun, F. Xu and L. Junkang, *Electrochim. Acta*, 2010, **55**, 4728–4733.